

On the regional-scale variability of flow duration curves in Peninsular India

Pankaj Dey¹, Jeenu Mathai², Murugesu Sivapalan^{3,4} and Pradeep. P. Mujumdar^{5,6}

¹Department of Hydrology, Indian Institute of Technology, Roorkee, India

²Marine Geoscience Group, National Centre for Earth Science Studies, Thiruvananthapuram, India

³Department of Civil and Environmental Engineering, University of Illinois at Urbana-Champaign, Urbana, IL, USA

⁴Department of Geography and Geographic Information Science, University of Illinois at Urbana-Champaign, Urbana, IL, USA

⁵Department of Civil Engineering, Indian Institute of Science, Bangalore, India

⁶Interdisciplinary Centre for Water Research, Indian Institute of Science, Bangalore, India

Correspondence to: Pankaj Dey (pdey609@gmail.com)

Abstract. Peninsular India is a unique region with major mountain ranges which govern regional atmospheric circulation and precipitation variability, the monsoons and regional geology at range of time and process scales. The controls of landscape and climatic features on streamflow variability at a regional scale using flow duration curve (FDC) – a compact description of streamflow variability, offering a window into the multiple, interacting processes that contribute to streamflow variability – is less explored. This study explores the suitability of partitioning of annual streamflow FDC into seasonal FDCs, and total streamflow FDC into fast and slow flow FDCs to unravel the process controls on FDCs at a regional scale, with application to low-gradient rivers flowing east from the Western Ghats of Peninsular India. The results indicate that bimodal rainfall seasonality and subsurface gradients explain the higher contribution of slow flow to total flow across north-south gradient of the region. Shapes of fast and slow FDCs are controlled by recession parameters revealing the role of climate seasonality and geologic profiles, respectively. A systematic spatial variation across north-south gradient is observed– highlighting the importance of coherent functioning of landscape-hydroclimate settings in imparting distinct signature of streamflow variability. The framework is useful to discover the role of time and process controls on streamflow variability in a region with seasonal hydro-climatology and hydro-geologic gradients. As each catchment responds uniquely, even when appearing similar, formulating generalizable hypotheses and using routinely employed signatures of catchment similarity to examine streamflow variability can be challenging. The Flow Duration Curve (FDC), offering a concise portrayal of streamflow variability at a specific gauging station, provides insights into hydroclimatic and landscape processes operating across a broad range of spatial and temporal scales that govern flow regimes in a region. This study delves into the controls of streamflow variability in Peninsular India, specifically focusing on low gradient rivers flowing east from the Western Ghats. The novelty of the study lies in partitioning streamflow into three time wise categories (non monsoon, southwest monsoon, northeast monsoon) and two process related partitions (fast flow and slow flow) using FDCs. The methodology enables a detailed examination of the contributions of each season and process to the overall annual flow. The study further enhances its novelty by accompanying an in-depth analysis of FDCs, incorporating a Mixed Gamma

~~Distribution (MGD) to model both fast and slow flow components. Uncovering the influence of climate, geology, and hydrological processes on MGD parameters, the study provides an advanced understanding of flow duration curve shapes. A key advancement is the integration of a comprehensive analysis of time scale decomposition, process decomposition, and statistical analyses, offering an in-depth exploration of streamflow variability controls in Peninsular India, contributing significantly to advancing our understanding of the complex interactions shaping streamflow patterns in the region.~~

1 Introduction

The hydrologic functioning of catchment systems in any given region is coevolved with the long-term climatology and landscape features present in the region through mutual interactions operating across multiple spatial and temporal scales (Wagener et al., 2013). These interactions and long-term feedbacks impart variability to hydrologic processes that are characteristic of the region of interest, including runoff generation and riverine transport processes, thus influencing water availability and reliability to human populations that depend on the streamflow. Understanding streamflow variability in time and space across river basins in the region is therefore very important for water resource management (Deshpande et al., 2016; Sinha et al., 2018) and the prediction and mitigation of floods (Kale et al., 1997). The frequency of high flows, low flows, or flows within specific ranges, is essential for risk assessment of water management projects involving control of streamflow variability. Correct portrayal of streamflow variability at the scale of catchments and river basins is therefore an indispensable component in many hydrologic applications.

The focus of this paper is on the flow duration curve (FDC), which is a compact description of temporal streamflow variability at the catchment scale. The FDC represents (daily) streamflow values plotted against the proportion of time the given flow is exceeded or equalled (Smakhtin, 2001; Vogel & Fennessey, 1994). The graphical form of the FDC embeds the governing hydrologic processes and dominant flow characteristics throughout the range of recorded streamflow at the catchment scale (Botter et al., 2008). In this sense, the FDC is also an important signature of a catchment's rainfall to runoff transformation (Ghotbi et al., 2020a; Vogel & Fennessey, 1994). FDC thus typifies the old proverb, "one picture is worth a thousand words" with its potential to encapsulate much of the relevant information of streamflow variability in a single plot (Vogel & Fennessey, 1995), and has been used in many hydrologic applications. Vogel and Fennessey (1994) provide a brief history of the application of flow duration curves in hydrology. Applications of FDC include waste load allocation (Searcy, 1959), water quality management (Searcy, 1959; Rehana & Mujumdar, 2011, 2012), reservoir and sedimentation studies (Vogel & Fennessey, 1995), low-flow and flood analyses (Smakhtin, 2001), assessment of environmental flow requirements (Smakhtin and Anputhas, 2006), and water availability for hydropower (Basso & Botter, 2012).

Streamflow observed in rivers results from the complex interplay of various hydrological processes, including runoff generation, overland and subsurface flow, and evaporation. These processes operate across multiple time and space scales, responding to climatic inputs and interacting with heterogeneous landscape properties. Deciphering the controls on streamflow variability and understanding their manifestation in the FDC shape pose significant challenges (Cheng et al., 2012; Ghotbi et al., 2020b; Yokoo & Sivapalan, 2011). Therefore, identifying

76 the process controls is essential to develop appropriate conceptual frameworks. This approach enables the
77 generation of profound insights into the governing principles that underpin the observed variability in catchments.

78 To address this complexity, Yokoo and Sivapalan (2011) proposed a conceptual framework for unravelling the
79 process controls of the FDC. They considered the Total Flow Duration Curve (TFDC) as a statistical summation
80 of a Fast Flow Duration Curve (FFDC) and a Slow Flow Duration Curve (SFDC). The FFDC, representing a
81 filtered version of precipitation variability, is influenced by rainfall intensity patterns and surface soil
82 characteristics. In contrast, the SFDC reflects the competition between subsurface drainage and
83 evapotranspiration, with seasonality and regional geology playing stronger roles (Yokoo & Sivapalan, 2011). This
84 distinction between fast (surface runoff) and slow (subsurface streamflow and groundwater flow) flow time scales
85 allows for a nuanced understanding of the process controls governing each component separately (Cheng et al.,
86 2012; Yokoo & Sivapalan, 2011).

87 Ghotbi et al (2020a, 2020b) used this framework to explore the climatic and landscape controls of FDCs using
88 streamflow data for hundreds of catchments across the continental United States in a comparative manner. In
89 their work Ghotbi et al. (2020a) emphasized the need to consider the fast flow and slow flow time series
90 independently as stochastic responses of catchments to sequences of storm events. Intensity and frequency of
91 rainfall events and the properties of soils and topography govern the variability of fast flows, whereas climate
92 seasonality and regional geology of the aquifer system govern variability of slow flow components. More
93 specifically, Ghotbi et al. (2020b) showed the dominant process controls of FDCs as aridity index, topographic
94 slope, coefficient of variation of daily precipitation, timing of rainfall, time interval between storms, snow fraction,
95 and recession slope.

96 Stewart (2015) introduces the Bump and Rise Method (BRM), a novel baseflow separation technique calibrated
97 with tracer data or optimization methods for accurate replication of tracer-determined baseflow shapes. The study
98 challenges the conventional practice of solely relying on streamflow for recession analysis, contending that it can
99 be misleading in understanding catchment storage reservoirs. The study also suggests for implementing baseflow
100 separation before recession analysis as a means to gain fresh insights into water storage reservoirs and potentially
101 resolve existing issues associated with recession analysis.

102 Significant advancements have been achieved in unravelling the process controls influencing flow duration
103 curves. However, challenges persist in extending this knowledge to large spatial scales. To address this, Leong
104 and Yokoo (2022) proposed an innovative approach, aiming to enhance the flexibility and adaptability of
105 hydrological models by transforming the representation of the subsurface component. This involves the creation
106 of a flexible structure composed of interconnected linear reservoirs, derived from a distinctive multiple
107 hydrograph separation procedure, offering a comprehensive interpretation of dominant processes impacting FDC
108 shapes and understand the number of distinct hydrological processes involved. In this study, we adopted the
109 method proposed by Ghotbi et al. (2020) and (2021) as a foundational step to characterize fast and slow flow
110 components, recognizing its inherent limitations stemming from its empirical and subjective nature.

111 Botter et al. (2008) addressed river basin streamflow variability by presenting a seasonal probability distribution
112 for daily streamflow using a stochastic soil moisture model. Extending this to the annual scale, the study
113 establishes analytical expressions for long-term flow duration curves, linking them to annual minima distribution

114 through key basin parameters, including climate, ecohydrology, and geomorphology. Muller et al. (2014) presents
115 a process-based analytical expression for flow duration curves in seasonally dry climates, employing a stochastic
116 model for wet season streamflow and a deterministic recession with stochastic initial conditions for the dry season.
117 The approach disentangles inter- and intra-annual streamflow variations effectively. Durighetto et al. (2022)
118 develops analytical expressions for flow duration curves and stream length duration curves (SLDC) to classify
119 streamflow and active length regimes in temporary rivers. It identifies two streamflow regimes (persistent and
120 erratic) and three active length regimes (ephemeral, perennial, and ephemeral de facto) based on dimensionless
121 parameters linked to streamflow fluctuations and catchment discharge sensitivity. The proposed framework,
122 validated in Italy and USA catchments, reveals a structural relationship between streamflow and active length
123 regimes, offering a promising tool for analysing discharge and river network length dynamics in temporary
124 streams.

125 Our approach to understanding spatial patterns across Peninsular India builds upon the foundational concept of
126 timescale decomposition, as previously explored in studies such as Botter et al. (2008), Muller et al. (2014), and
127 Durighetto et al. (2022). The decomposition of timescales, while not novel in our study, serves as a fundamental
128 framework, aiding our analysis of spatial dynamics in the region.

~~129 The novelty of the paper lies in exploring the controls of streamflow variability in Peninsular India, a result of the
130 impacts of monsoons—southwest (summer season) and northeast (winter season), the presence of western and
131 eastern ghats, and topographical gradients. The paper advances the field by partitioning streamflow into three
132 distinct time-wise categories (non-monsoon, southwest monsoon, and northeast monsoon) and two process-wise
133 partitions (fast flow and slow flow), using flow duration curves as a tool. This approach allows for a detailed
134 examination of the relative contributions of each season and process to the overall annual flow.~~

~~135 Furthermore, the integration of a comprehensive approach to analysing flow duration curves by incorporating a
136 Mixed Gamma Distribution (MGD) to model both fast and slow flow components, along with seasonal and
137 regional exploration, enhances the study's novelty, and the study uncovers the influence of climate, geology, and
138 hydrological processes on MGD parameters, providing a better understanding of flow duration curve shapes. The
139 inclusion of links between MGD parameters and landscape properties, as well as the association between the
140 midsection slope of the FDC and recession parameters, adds an additional layer of sophistication to the analysis.
141 This provides a more robust understanding and offers insights into spatial variations, highlighting the integrated
142 role of surface and subsurface processes in shaping the catchment's average flow regime~~

~~143 The study stands out for its innovative combination of time scale decomposition, process decomposition, and
144 statistical analyses, offering a holistic exploration of the controls of streamflow variability in Peninsular India.
145 The partitioning approach and the integration of statistical analysis contribute significantly to advancing our
146 understanding of the complex interactions shaping streamflow patterns in this region. We recognize the abundance
147 of literature in FDC studies, but we believe our contribution is valuable in providing a detailed understanding of
148 the controls on streamflow variability in the context of Peninsular India.~~

149 Leong and Yokoo (2022) introduced an innovative approach, employing interconnected linear reservoirs to
150 enhance hydrological model flexibility and adaptability. Carlier et al. (2018) addressed the neglect of geological
151 characteristics in catchment studies, revealing that climate conditions predominantly influence medium to high

152 discharge percentiles, while the catchment's ability to buffer meteorological forcing is attributed to geological
153 features. Botter et al. (2013) identified an index incorporating climate and landscape attributes to discriminate
154 between erratic and persistent flow regimes, providing a robust framework for characterizing hydrology in the
155 face of global change. Basso et al. (2015) investigated the role of non-linear storage–discharge relations in shaping
156 high-flow distributions, emphasizing the importance of analysing individual events for accurate characterization.
157 Ye et al. (2012) explored regional variations in streamflow regime behaviour across the U.S., highlighting the
158 significance of snowmelt, vegetation cover dynamics, and climate trends. Fenicia et al. (2014) linked perceptual
159 hydrological models with mathematical structures, demonstrating how distinct catchment processes influence
160 model performance and emphasizing the need to synthesize experimentalist and modeler perspectives. Together,
161 these studies contribute to a comprehensive understanding of FDCs and advance our knowledge of hydrological
162 processes at different scales.

163 While the existing literature, represented by studies such as Leong and Yokoo (2022), Carlier et al. (2018), Botter
164 et al. (2013), Basso et al. (2015), Ye et al. (2012), and Fenicia et al. (2014), has made significant strides in
165 understanding the controls of flow duration curves and streamflow variability, our study distinguishes itself by
166 focusing on the unique hydrological context of Peninsular India. The previously discussed works have primarily
167 addressed FDC drivers at regional or global scales, examining factors such as hydrogeology, climate, and
168 landscape alterations. In contrast, our study delves into the specific challenges posed by the Peninsular Indian
169 environment, characterized by the interplay of monsoons, mountainous terrain, and topographical gradients.
170 Through a comprehensive approach encompassing time scale decomposition and process decomposition, and
171 statistical analyses, we employ FDC as a key tool to unravel the controls of streamflow variability across
172 Peninsular India. Our work enhances the understanding of hydrological processes in a region with distinct
173 monsoonal influences, thus advancing the state of the art and providing valuable insights for water resource
174 management in Peninsular India.

175 The novelty of the paper lies in exploring the controls of streamflow variability in Peninsular India, a result of the
176 impacts of monsoons – southwest (summer season) and northeast (winter season) – the presence of western and
177 eastern ghats, and topographical gradients. The paper advances the field by partitioning streamflow into three
178 distinct time-wise categories (non-monsoon, southwest monsoon, and northeast monsoon) and two process-wise
179 partitions (fast flow and slow flow), using flow duration curves as a tool. This approach allows for a detailed
180 examination of the relative contributions of each season and process to the overall annual flow. Furthermore, the
181 integration of a comprehensive approach to analyzing flow duration curves by incorporating a Mixed Gamma
182 Distribution (MGD) to model both fast and slow flow components, along with seasonal and regional exploration,
183 enhances the study's novelty. The study uncovers the influence of climate, geology, and hydrological processes
184 on MGD parameters, providing a better understanding of flow duration curve shapes. The inclusion of links
185 between MGD parameters and landscape properties, as well as the association between the midsection slope of
186 the FDC and recession parameters, adds an additional layer of sophistication to the analysis. We recognize the
187 abundance of literature in FDC studies, but we believe our contribution is distinctive due to its innovative
188 combination of partitioning techniques and statistical analysis, offering deeper insights into spatial variations and
189 emphasizing the intertwined influence of surface and subsurface processes on streamflow patterns in the region.

190 The remainder of the paper is structured as follows. Section 2 elaborates on the details of the study area and the
191 daily streamflow dataset used. The description of the methodology employed for the analysis is presented in
192 Section 3. The results of the application of the framework to Peninsular India and the interpretation of the results
193 are presented in Sections 4 and 5, respectively. Finally, the paper is concluded in Section 6 with key insights
194 gained for the nature and controls of streamflow variability across Peninsular India.

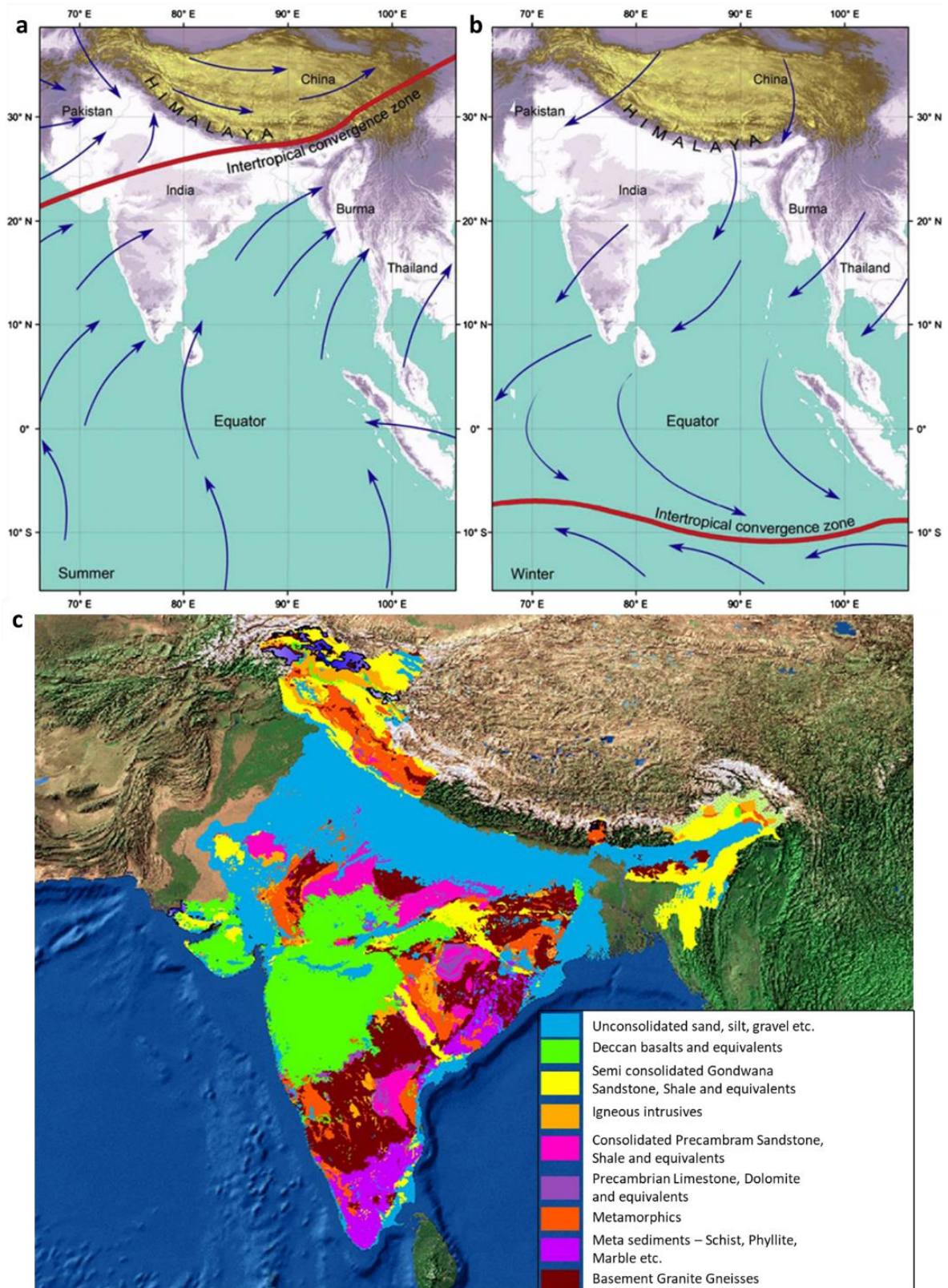
195 **2 Study region**

196 Peninsular India is a cratonic region with an approximate shape of a vast inverted triangle with diverse topography
197 and characteristic climatic patterns, bounded by the Arabian Sea in the west, the Bay of Bengal in the east, and
198 the Vindhya and Satpura ranges in the north. The long escarpments of the Western Ghats and the Eastern Ghats,
199 constituting the western and eastern continental fringes of India, and an asymmetric relief with eastward tilt
200 towards the floodplains of several eastward draining rivers from the 1.5 km high Western Ghats, characterize the
201 physiography of Peninsular India (Richards et al., 2016). The rise of the Himalayan-Tibetan plateau has
202 significantly contributed to the Neogene climate of Asia, favoured the birth of the modern monsoon (Fig. 1.a, b)
203 (Chatterjee et al., 2013, 2017), and triggered glaciation in the Northern region. A wide variety of plateaux, open
204 valleys, bedrock gorges, mountain ranges, inselbergs and residual hills constitute the geomorphology of
205 Peninsular India (Kale & Vaidyanadhan, 2014). The Peninsular landscape is dominated by Deccan Traps (Deccan
206 basalts) of Cretaceous-Eocene, igneous and metamorphic rocks (Granite-gneisses) of Archaean-Late Precambrian
207 along with minor consolidated sediments (Sandstone, shale) of Precambrian-Jurassic (Fig. 1.c) (Kale, 2014).

208 The region is strongly impacted by monsoons, major seasonal winds which are a manifestation of the seasonal
209 movement of the Intertropical Convergence Zone (ICTZ in Fig. 1.a and Fig. 1.b), which contribute largely to the
210 annual rainfall variability in much of the Indian subcontinent (Gadgil, 2003). The monsoons have two components
211 – South-West monsoon and North-East monsoon, which arrive during June – September (JJAS) and October –
212 December (OND), respectively. South-West monsoon season contributes more than 75% of annual rainfall over
213 majority of the regions of the country (Saha et al., 1979). However, the Southern Peninsula receives a significant
214 portion (30-60%) of its annual rainfall during the North-East monsoon, which contributes only 11% of the rainfall
215 annually to India as a whole (Rajeevan et al., 2012). The maximum extent of rainfall over the Southern Peninsula
216 during the North-East Monsoon is due to the reversal of lower-level winds over South Asia from the South-West
217 to the North-East during the retreating phase of the South-West monsoon (Rajeevan et al., 2012). Peninsular India
218 displays south-to-north variability in the South-West monsoon, causing heavy rainfall along the Western Ghats
219 and reduced amounts in the central and northeastern regions (Fig S2.a in Supplementary Material).

220 The Western Ghats' long escarpment hosts predominantly tropical evergreen forest, crucial for intercepting South-
221 West monsoon winds (Ramachandra, 2018). Ramachandra (2018) depicted a west-east vegetation gradient along
222 the Western Ghats, transitioning from tropical-evergreen to semi-evergreen and progressing to moist to dry
223 deciduous forests towards the rain-shadow region in the east. The topography map for the Peninsular region and
224 a selected point in the region is depicted in Fig. S1.a and Fig. S1.b in Supplementary Material, respectively. The
225 western margin of Peninsular India, influenced by the Western Ghats, receives heavy rainfall, while the rain
226 shadow region experiences deficient rainfall (Fig. S2.c). The geological and tectonic history, coupled with
227 monsoon climate events, has significantly shaped the present landform (Kale, 2014).

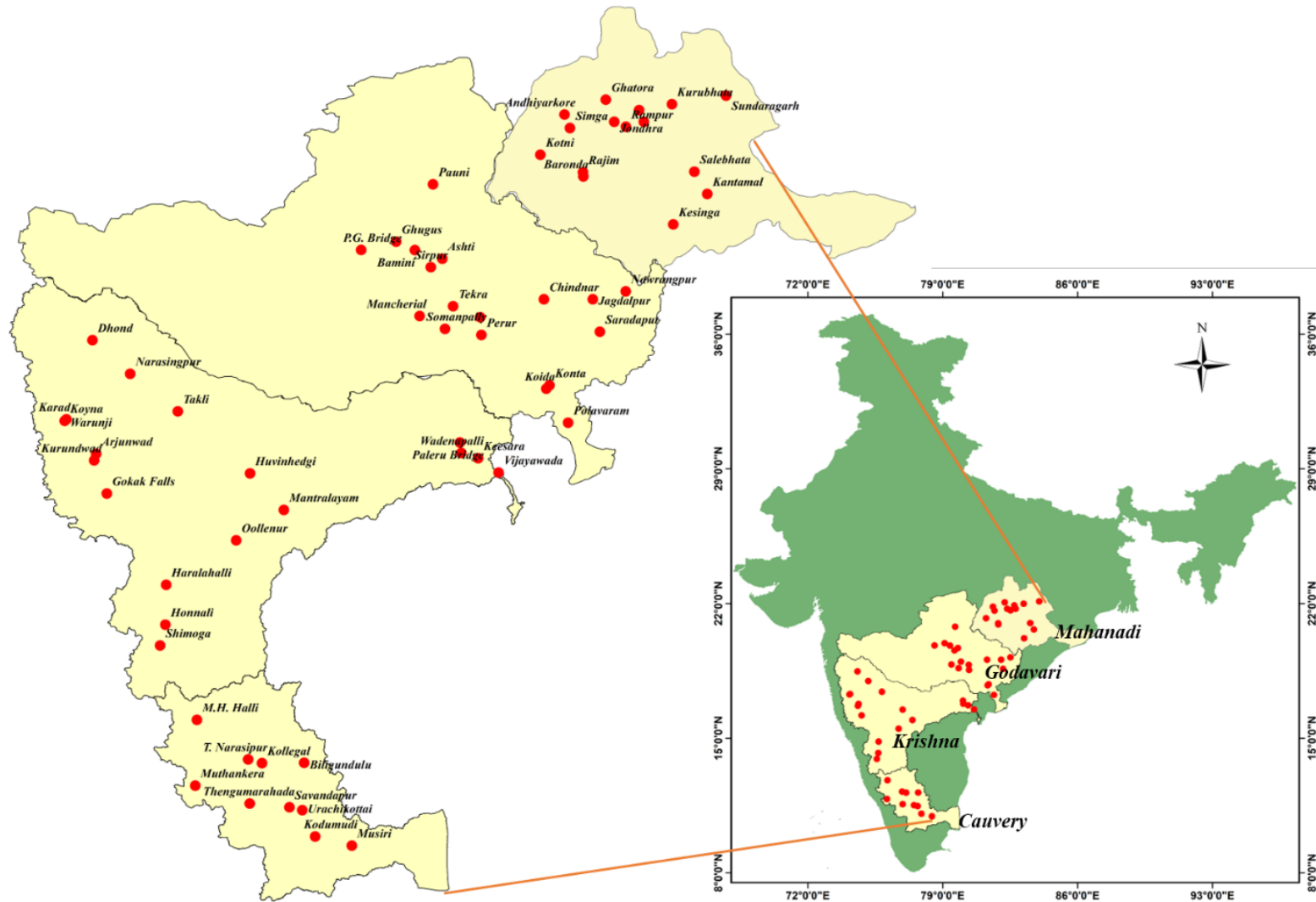
228 The region shown in Fig. 2 is selected as the study area in the Deccan Plateau of Peninsular India. The escarpment
229 of Western Ghats forms the western margin of the Deccan Plateau which serves as the main water divide for the
230 Peninsular River systems. The gentle slope from west to east causes Peninsular rivers such as the Mahanadi,
231 Godavari, Krishna, and Cauvery (Fig. 2) to flow eastwards. Three of these rivers (Godavari, Krishna and Cauvery)
232 originate from the Western Ghats, spread across the area from the Deccan Plateau, flow eastwards, and drain into
233 the Bay of Bengal. The Mahanadi River rises in the mountains of Siwaha bounded by the Eastern Ghats in the
234 south and east, and drain eastwards into the Bay of Bengal. Additional details about the river basins can be found
235 in Text T1 within the Supplementary Information. The study utilizes daily streamflow data (1965-2012) from 62
236 gauges across four river basins, sourced from the Water Resources Information System (WRIS) database. Analysis
237 incorporates a daily gridded rainfall product ($0.25^\circ \times 0.25^\circ$) from the India Meteorological Department (Pai et al.,
238 2014).



239

240 **Figure 1.** (a) The relation of uplift of Himalaya-Tibetan Plateau and monsoon initiation in India. Monsoon winds
 241 blow from the Indian Ocean towards land in the summer (b) during the winter, the Himalaya prevents cold air
 242 from passing into the subcontinent and causes the reversal of wind direction and monsoon blow from land toward
 243 sea [Reprinted from (Chatterjee et al., 2013)] (c) geology of Peninsular India [Reprinted from: Central Ground
 244 Water Board(<https://www.aims-cgwb.org/general-background.php>)].

245



246
 247
 248 **Figure 2.** Location map of four Peninsular River Basins. Stream gauges considered in this study are marked with red circles.

249 3 Methodology

250 Initially, the study employs time scale partitioning to analyse flow duration curves across Peninsular India,
251 focusing on Non-monsoon, South-West monsoon, and North-East monsoon periods in four river basins. The
252 analysis extends to regional scales, encompassing streamflow time series from all gauging stations, and includes
253 process scale partitioning to assess the relative contributions of fast and slow flow components, revealing spatial
254 patterns influenced by climate, geology, and aquifer characteristics.

255 Additionally, the methodology entails a comprehensive analysis of FDCs for fast and slow flow components
256 across seasons. It includes scaling time series to remove the influence of mean climate and geology, utilizing the
257 statistical distributions to examine parameters influencing FDC shapes. The study explores links between
258 statistical parameters and landscape properties through recession analysis and investigates spatial variation in
259 FDC parameters using descriptors such as latitude, longitude, and catchment area. The final part of the
260 methodology focuses the association between the midsection slope of the FDC and recession parameters,
261 exploring the role of both surface and subsurface processes in controlling the average flow regime of the
262 catchment.

263 3.1 Time Scale Partitioning

264 The streamflow hydrograph, representing a catchment's response to random rainfall events, is treated as a
265 stochastic time series, with streamflow considered a random variable. Utilizing distribution functions like the
266 cumulative distribution function (CDF) allows for a concise assessment of streamflow variability, aiding in the
267 interpretation and comparison of catchment responses. CDFs have diagnostic and practical value, facilitating the
268 classification of catchments based on flow regimes and supporting probabilistic treatments in engineering design
269 and environmental monitoring. The cumulative distribution function of a random variable (the random variable
270 of interest to us is daily streamflow; Q) expresses the probability that a realization (i.e., observation) of Q does
271 not exceed a specific value q .

272 The flow duration curve, an equivalent measure of streamflow variability, represents the fraction of time (D) that
273 streamflow is likely to equal or exceed a specified value, expressed mathematically as,

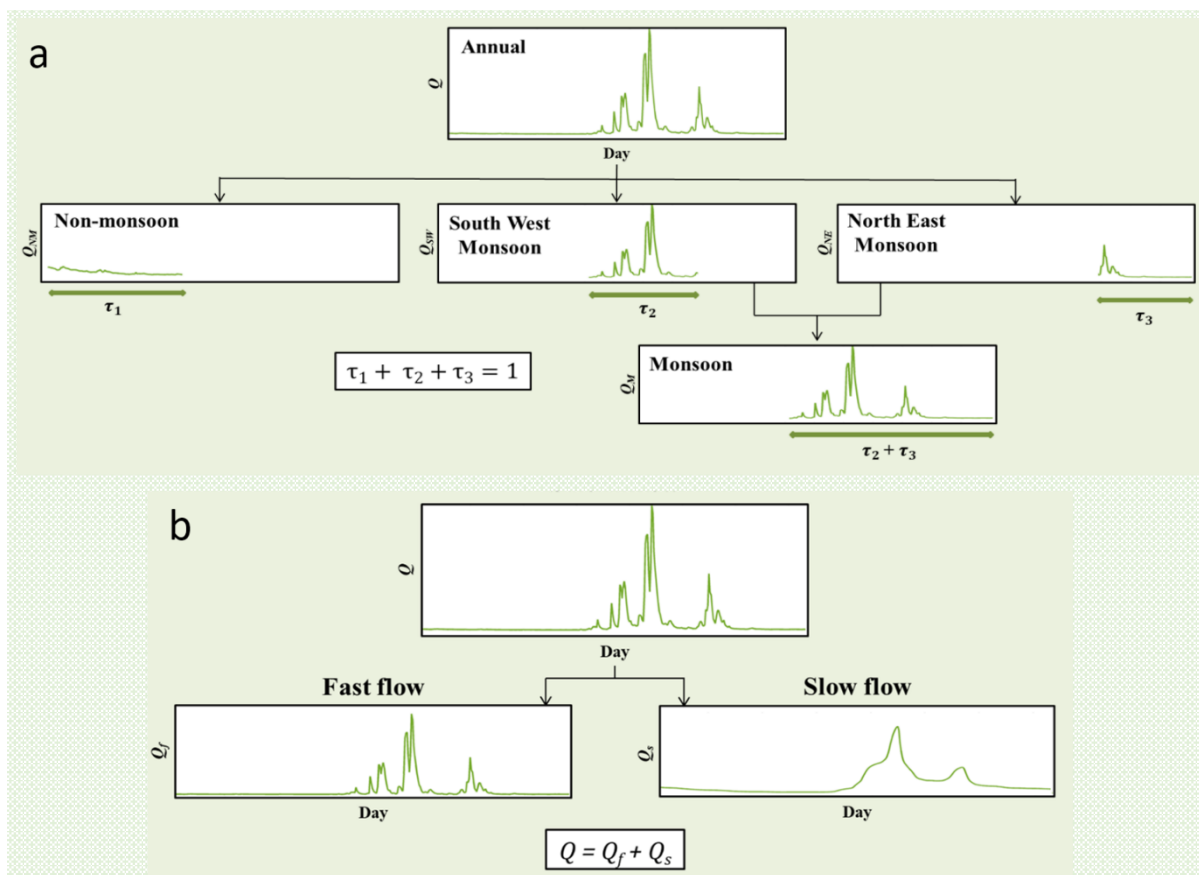
$$D(q) = P[Q \geq q] = 1 - F(q) \quad (1)$$

274 Despite its probabilistic definition, the flow duration curve is commonly plotted in hydrological applications as
275 $q(D)$, i.e., q (in the vertical axis) as a function of D (in the horizontal axis).

276 The streamflow time series can be equivalently divided into temporal segments of distinct seasons as well as
277 distinct months. In this case, by joining observed time series over multiple years, FDCs for each time segment can
278 be reconstructed. Assuming independence (as an approximation), these can then be combined to generate annual
279 FDCs. The theory for the time scale partitioning is illustrated in Fig. 3a. The year is divided into three distinct
280 (non-overlapping) seasons, viz. Non-monsoon, South-West, and North-East seasons (for Peninsular India) of

281 relative durations τ_1 , τ_2 , and τ_3 (with $\tau_1 + \tau_2 + \tau_3 = 1$) respectively. These seasons can be assumed to have
 282 distinct characteristics in terms of rainfall variability and how they translate to streamflow variability. The daily
 283 streamflow time series is used to construct the seasonal as well as annual FDCs. For example, the FDC of Non-
 284 monsoon season is constructed by using the daily streamflow during the period of January – May over the years.
 285 Similarly, FDCs for South-West and North-East monsoons are constructed using the daily streamflow during June
 286 – September and October – December months over the years respectively and the annual FDC is constructed using
 287 daily streamflow values for 365/366 days over the years. The FDCs at monthly time scales are obtained using the
 288 daily values of streamflow in a month over the years. The FDCs for the three distinct seasons, i.e., Non-monsoon,
 289 South-West monsoon, North-East monsoon, are denoted as $D_{NM}(q)$, $D_{SW}(q)$, and $D_{NE}(q)$ respectively. Initially,
 290 the FDCs for each season can be constructed separately (Fig. 3a).

291



292

293 **Figure 3. Time and process scale partitioning. a)** Scale partitioning into seasonal and monthly time scales. The
 294 conceptual framework illustrates the time scale partitioning of streamflow time series into various seasonal
 295 components considering patterns of rainfall variability. The annual streamflow time series is decomposed into
 296 three components: (1) Non-monsoon flow, (2) South-West monsoon flow, and (3) North-East monsoon flow. **b)**
 297 The schematic representation illustrates the process partitioning of streamflow time series into the fast flow and
 298 slow flow components.

299 The annual FDC with exceedance probability $P [Q \geq q]$ refers to the probability of flow in annual scale being
 300 greater than or equal to q , and is expressed as

$$D(q) = P [Q \geq q] = \tau_1 P_{(NM)} [Q \geq q] + \tau_2 P_{(SW)} [Q \geq q] + \tau_3 P_{(NE)} [Q \geq q] \quad (2)$$

$$\text{or, } D(q) = \tau_1 D_{NM}(q) + \tau_2 D_{SW}(q) + \tau_3 D_{NE}(q) \quad (3)$$

301 where, $P_{(NM)} [Q \geq q]$, $P_{(SW)} [Q \geq q]$ and $P_{(NE)} [Q \geq q]$ refer to, respectively, the probability of flow in Non-
 302 monsoon, South-West monsoon and North-East monsoon being greater than q . As the seasons are nonoverlapping
 303 the probability of flow being greater than q at annual scale (i.e., $P [Q \geq q]$) can be expressed as the sum of the
 304 weighted probabilities of flow being greater than q in the three seasons.

305 In general, the FDC at the annual scale can be constructed as follows:

$$D(q) = \tau_1 D_1(q) + \tau_2 D_2(q) + \dots + \tau_n D_n(q) \quad (4)$$

306 where n is the number of distinct seasons considered for the analysis and, $\tau_1 + \tau_2 + \dots + \tau_n = 1$. The validity of
 307 the above depends on the assumption that there is no carryover of flows from one season to the next season (which
 308 is an approximation). In this study, the assumption of independence between flows across three seasons is checked
 309 using multivariate Hoeffding's test (see details in Text T2 of Supplementary Information).

310 The relative contributions of Non-monsoon ($C_{NM \rightarrow AN}$), South-West monsoon ($C_{SW \rightarrow AN}$) and North-East monsoon
 311 ($C_{NE \rightarrow AN}$) flows to annual flow can be approximated through following expressions:

$$C_{NM \rightarrow AN} = \frac{\tau_1 E(Q_{NM})}{\tau_1 E(Q_{NM}) + \tau_2 E(Q_{SW}) + \tau_3 E(Q_{NE})} \quad (5)$$

$$C_{SW \rightarrow AN} = \frac{\tau_2 E(Q_{SW})}{\tau_1 E(Q_{NM}) + \tau_2 E(Q_{SW}) + \tau_3 E(Q_{NE})} \quad (6)$$

$$C_{NE \rightarrow AN} = \frac{\tau_3 E(Q_{NE})}{\tau_1 E(Q_{NM}) + \tau_2 E(Q_{SW}) + \tau_3 E(Q_{NE})} \quad (7)$$

312 Similarly, the relative contributions of monthly flows to annual flow can be expressed as:

$$C_{m \rightarrow AN} = \frac{\frac{1}{12} E(Q_m)}{\frac{1}{12} \sum_{m=1}^{12} E(Q_m)} \quad (8)$$

313 Note, as before, these relative contributions to total flow effectively also measure the relative contributions of the
 314 seasonal/monthly flows to the mean of the annual flow duration curve.

315 The methodology for constructing annual FDC using seasonal FDC is as follows:

316 1. The empirical PDFs – $f_{NM}(q)$, $f_{SW}(q)$ and $f_{NE}(q)$ are derived for daily streamflow time series for Non-
 317 monsoon, South-West monsoon and North-East monsoon seasons respectively.

318 2. These PDFs are then multiplied by scaling factors, τ_1 , τ_2 and τ_3 in equation S4. The scaling factors represent
 319 relative durations of the three seasons considered. For example, $\tau_1 = 5/12$, as the duration of duration of non-
 320 monsoon season is 5 months.

321 3. The PDF of annual flow is estimated as the weighted sum of three scaled density functions corresponding to
 322 three seasons (see Eq. S2). The annual flow consists of the daily streamflow for Non-monsoon, South-West
 323 monsoon and North-East monsoon seasons.

324 The performance of the time scale partitioning framework is assessed using the metric, root mean square error
 325 (RMSE). The method of estimation of q_{sim} is shown in Fig. S3.

$$326 \quad RMSE = \sqrt{\frac{1}{n} \sum_{i=1}^n (q_{actual} - q_{sim})^2} \quad (9)$$

327 **3.2 Process Partitioning**

328 Daily streamflow is partitioned in such a way that it approximates the statistical summation of fast flow and slow
 329 flow at the daily scale (Fig.3b):

$$Q = Q_f + Q_s \quad (10)$$

330 where Q is the daily streamflow, Q_f is the daily fast flow, Q_s is the daily slow flow.

331 The relative contributions of fast flow ($C_{\rightarrow TF}$) and slow flow ($C_{SF \rightarrow TF}$) to total flow can be expressed as

$$C_{Q_f \rightarrow Q} = \frac{\text{Total Fast Flow Volume}}{\text{Total Flow Volume}} \quad (11)$$

$$C_{Q_s \rightarrow Q} = \frac{\text{Total Slow Flow Volume}}{\text{Total Flow Volume}} \quad (12)$$

332 Note that $C_{Q_f \rightarrow Q}$ and $C_{Q_s \rightarrow Q}$ effectively measure the relative contributions of fast and slow flows to the mean of
 333 the annual flow duration curve.

334 **3.3 Exploring Controls and Spatial Patterns of Flow Duration Curves: Insights from Statistical Distributions** 335 **and Analysis of Mid-Section Slope**

336 The analysis then extends to the comprehensive analysis of flow duration curves for fast and slow flow
 337 components across different seasons, with a focus on understanding their variations and controls. The first step is
 338 to scale the fast and slow flow time series by their respective long-term mean values, effectively removing the
 339 influence of mean climate and geology. This scaling allows the identification of secondary controls on the shapes
 340 of FDCs.

341 The Mixed Gamma Distribution (MGD) is then used to fit the scaled fast and slow flow time series, and the
 342 parameters of the MGD are examined for their influence on the FDC shapes (see text T4 of Supplementary

343 Information) Krasovskaia et al., 2006; Botter et al., 2007; Muller and Thompson 2016; Santos et al., 2018. The
344 variation of the parameters of the MGD are explored, regionally and seasonally, considering the influence of mean
345 climate, geology, and complex hydrological processes on fast and slow flows. The performance of the MGD in
346 fitting FDCs is assessed using goodness-of-fit metrics such as the Nash-Sutcliffe efficiency (NSE) and coefficient
347 of determination (R^2). Seasonal variations of MGD parameters are analysed at a regional scale, considering all
348 gauging stations. ~~The study further explores the link between MGD parameters and landscape properties through~~
349 ~~recession analysis. The studies by Botter et al. (2013), Muller et al. (2014), Basso et al. (2015), Arai et al. (2021),~~
350 ~~Leong and Yokoo (2022; 2019) collectively enhance understanding of the intricate relationship between recession~~
351 ~~parameters and FDC characteristics. They emphasize the significant influence of recession parameters on~~
352 ~~hydrological regimes, catchment scale attributes, non-linear storage discharge relations, and the practical~~
353 ~~applications in predicting FDCs, showcasing a comprehensive exploration of the pivotal role these parameters~~
354 ~~play in shaping hydrological responses at various spatial scales. Leong and Yokoo (2022) innovative modeling of~~
355 ~~subsurface components further contribute to a deeper comprehension of the dominant processes influencing FDC~~
356 ~~shapes. The studies conducted by Botter et al. (2013), Muller et al. (2014), Basso et al. (2015), Arai et al. (2021),~~
357 ~~and Leong and Yokoo (2022; 2019) illuminate the complex interplay between recession parameters and FDC~~
358 ~~characteristics, underscoring the pivotal influence of recession parameters on hydrological systems, encompassing~~
359 ~~catchment attributes and storage-discharge relationships. Consequently, in pursuit for deeper understanding, we~~
360 ~~delve into examining the connection between MGD parameters and landscape properties via recession analysis.~~
361 Spatial variation in FDC parameters is then investigated using descriptors such as latitude, longitude, and
362 catchment area.

363 The final aspect of the methodology involves the association between the midsection slope of the FDC and
364 recession parameters, emphasizing the role of both surface and subsurface processes in controlling the average
365 flow regime of the catchment. The methodology aims to unravel the intricate interplay of climate, geology, and
366 hydrological processes in shaping the regional hydrologic signatures of Peninsular India.

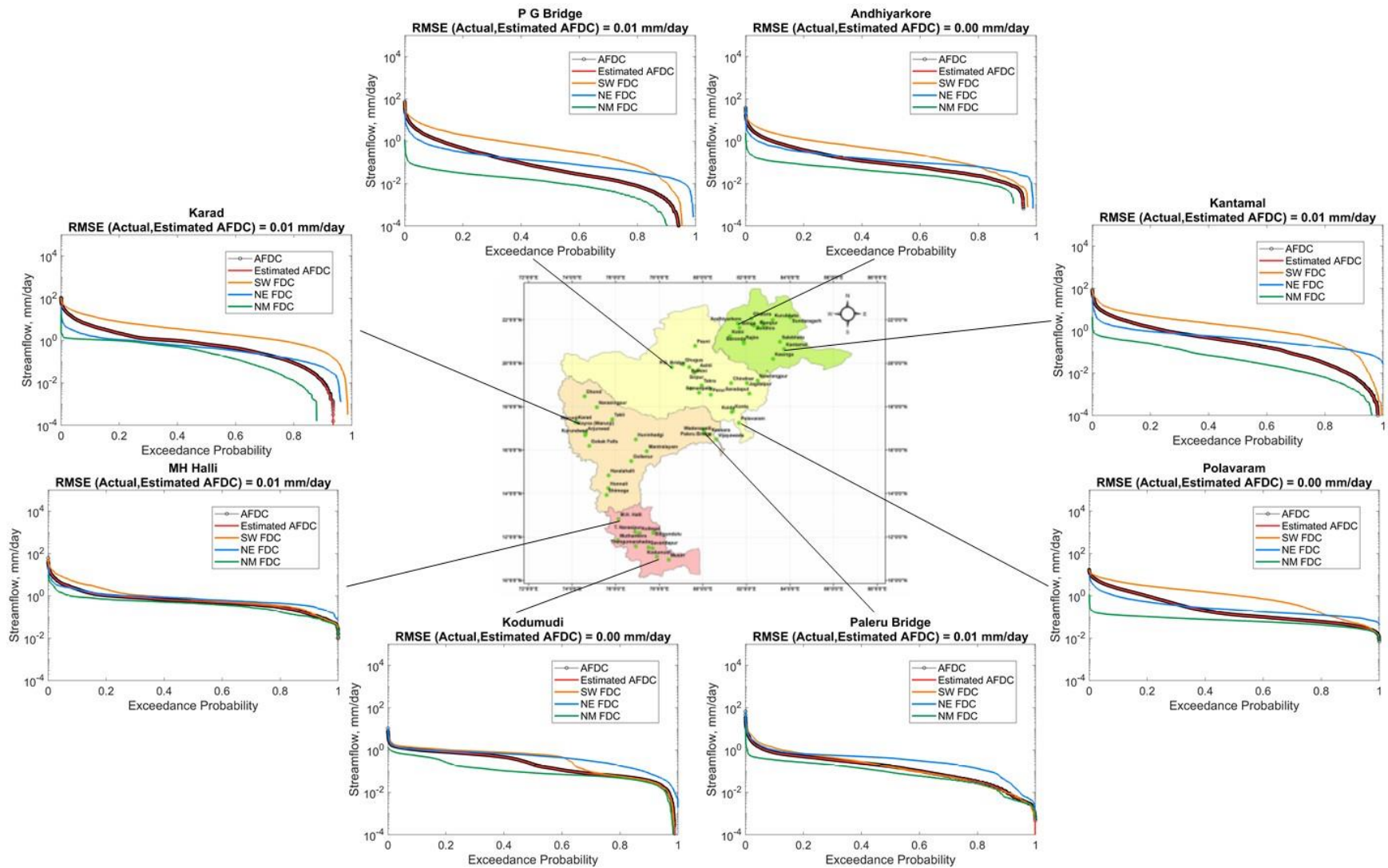
367 **4 Results and Discussions**

368 **4.1 Time scale partitioning**

369 We initially investigated the spatial variations in seasonal and annual flow duration curves across Peninsular India
370 employing the partitioning framework. The annual flow duration curve and seasonal flow duration curves for
371 Non-monsoon, South-West monsoon, and North-East monsoon are shown in Fig. 4 for eight representative
372 gauges, one at the upstream and one at the downstream of each of the four river basins. The estimated annual flow
373 duration curve (red curve) using equation S2 is also shown in Fig. 4. Daily streamflow time series is normalized
374 by catchment area before plotting (on a semi-log paper) the flow duration curve for comparison across the gauging
375 stations. In particular, the annual flow duration curve (black scatter) is reproduced well by the partitioning of both
376 seasonal (red curve in Fig. 4) and monthly flows (red curve in Fig. S4). The mean and variance of annual flows
377 are also reproduced well by the time scale partitioning framework (Fig. S5). This confirms the efficacy of the time
378 scale partitioning approach of seasonal/monthly flows in approximating the annual flow duration curve (see also
379 Fig. S4, Fig. S5.a and Fig. S5.d in Supplementary Material).

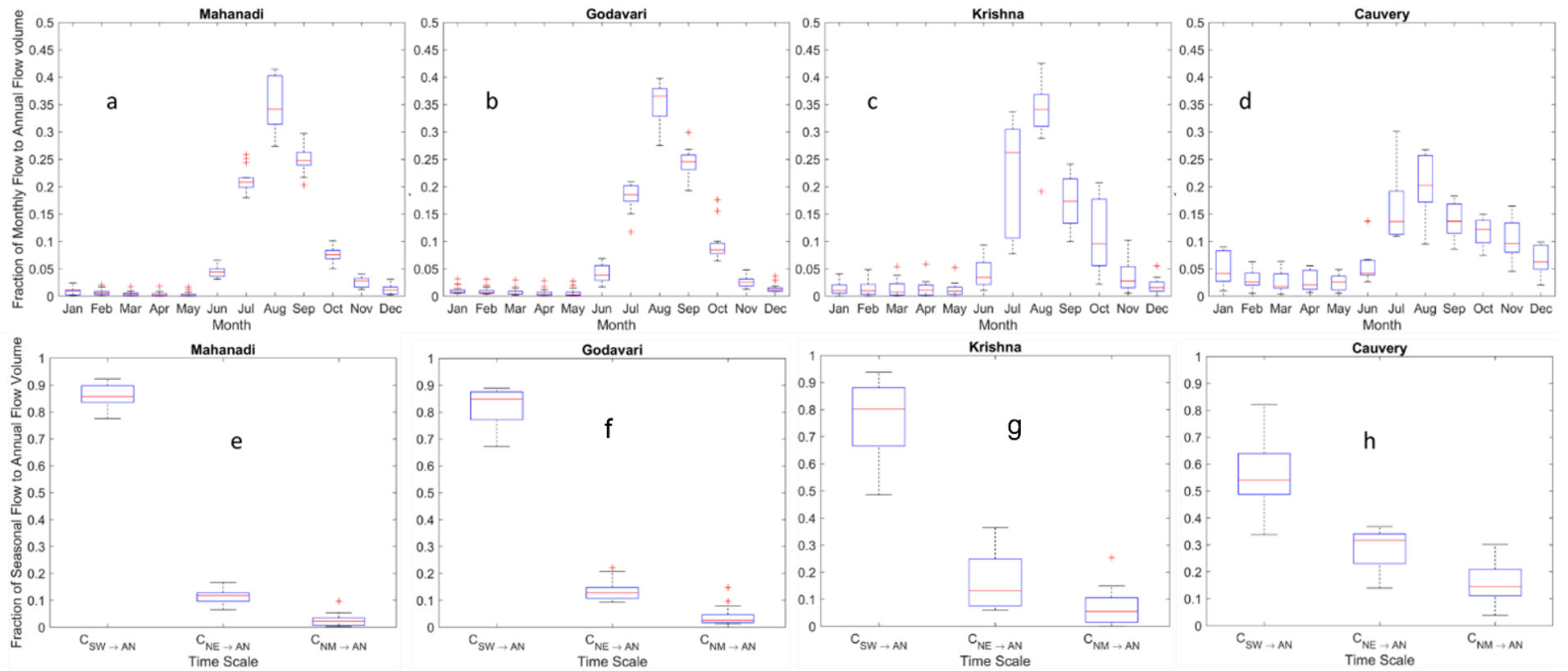
380 Another feature that can be observed in Fig. 4 is that in gauging stations located in the northern part of the
381 peninsular region, flow duration curves (FDCs) of South-West monsoon flows (orange curve) are relatively higher
382 than other seasonal FDCs. Given the logarithmic scale used to plot the flows, this dominance is significant. In
383 sites located in the southern part of the region, the dominance of South-West monsoon is not as strong and North-
384 East monsoon flows (blue curve) are also significant.

385 Motivated by these observations, we extracted seasonal and monthly streamflow time series from the entire dataset
386 across all gauging stations to compute the relative contributions of seasonal and monthly flows to the annual flow
387 duration curve. The results are presented in Fig. 5. At the monthly scale (top panel, Fig. 5), the contributions of
388 flows during the months of June to September are much higher than in other months in northern Peninsular basins
389 (Mahanadi and Godavari, Krishna to a less extent). This can be explained by the contribution of monthly rainfall
390 to annual rainfall, which is higher during these months as shown in Fig. S6. On the other hand, in the southernmost
391 Cauvery basin, the dominance of June to September months is relatively not as strong, and there is also a
392 significant contribution during the months of October to December, higher than in northern basins (Fig. 5.d). This
393 can be attributed to the slightly more equal dominance of both South-West (June - September) and North-East
394 (October – December) monsoons over the Cauvery basin (Fig. S6.d) than in the northern basins. This pattern is
395 also reflected at the seasonal scale (bottom panel, Fig. 5), with the contribution of South-West monsoon flow to
396 annual flow being slightly higher than that during the other seasons, and much higher in northern basins. However,
397 the contribution of South-West monsoon to annual flow decreases in southern basins, while the contribution of
398 North-East monsoon increases, as can be seen clearly in Fig. 5.h for the Cauvery basin. The contribution of Non-
399 monsoon to annual flow is also higher in southern basins relative to northern basins. This can be attributed to
400 carry over flows from winter rains during the North-East monsoon, which is more pronounced in the southern
401 part of the region.



402

403 **Figure 4.** Spatial variations in seasonal and annual flow duration curves across Peninsular India. The time scale partitioning framework of seasonal flows in approximating
 404 annual flow duration curves works reasonably well.



405

406

407

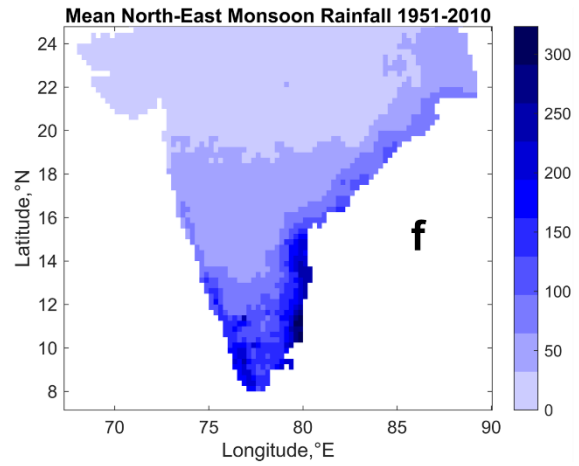
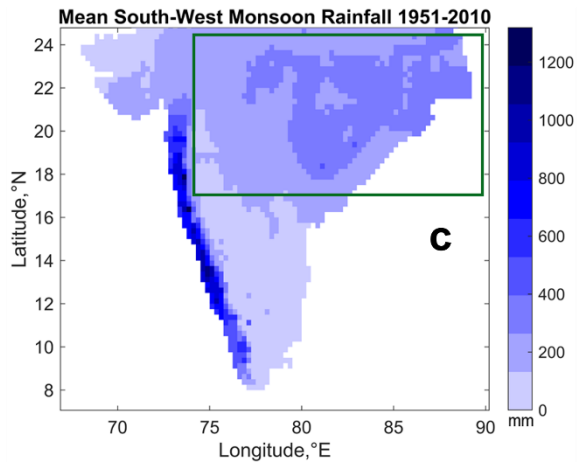
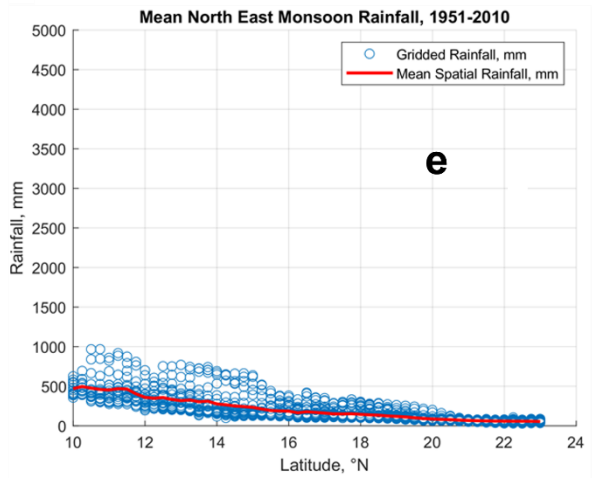
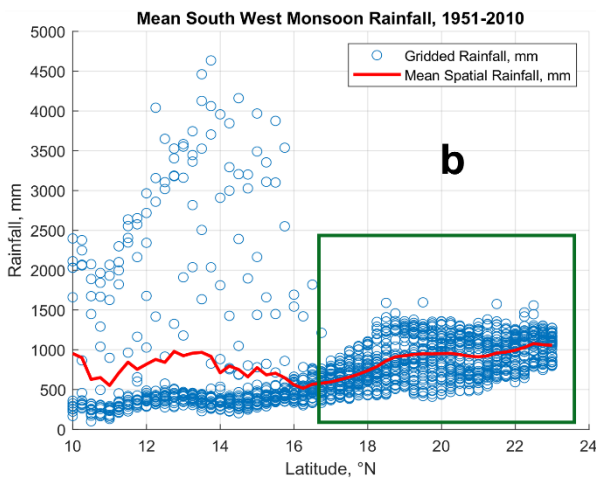
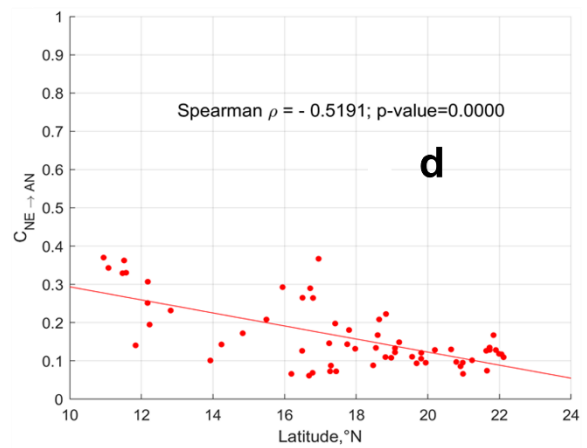
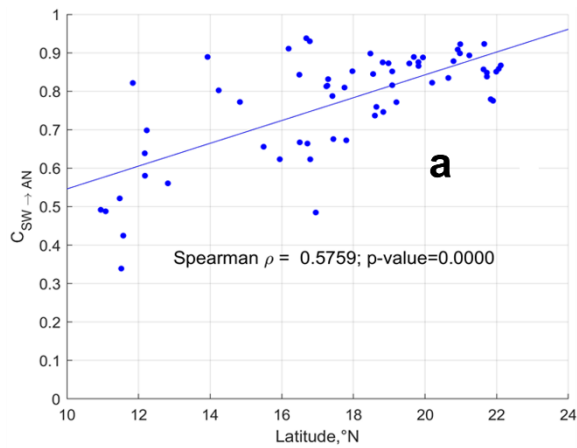
Figure 5. The relative contributions of monthly and seasonal flows to annual flow at basin scale. The contributions of South-West monsoon flow to annual flow increases in northern basins whereas it decreases in southern basins. However, the contributions of North-East monsoon flow to annual flow increases towards southern basins.

408 We next carried out regional scale analysis by considering streamflow time series of all the gauging stations across
409 all four river basins. Similar to basin scale analysis presented before, the relative contributions of seasonal and
410 monthly flows to annual flow are now estimated at the regional scale (Fig. 6). The spatial patterns of South-West
411 and North-East monsoon rainfall across the Peninsular region are plotted for comparison using IMD gridded
412 rainfall product (Fig. 6.b and Fig. 6.e).

413 The contribution of South-West monsoon flows to annual flow increases in the northerly direction (Fig. 6.a). The
414 mountainous region of the southern Peninsula (western part of Krishna basin and north-western part of Cauvery
415 basin) receives high rainfall during the South-West monsoon season (Fig. 6.b – extended till 17° N latitude). The
416 streamflow produced in the headwater regions of southern basins in response to high rainfall, contributes at least
417 70% of the annual flow (Fig. 6.a). Yet, the areal fraction of these high rainfall, headwater regions within the four
418 river basins is quite small and their contributions to the average precipitation or flow at the basin scale is much
419 smaller. There is also considerable variability in the contributions of South-West monsoon flows to annual flow
420 in the sub-basins located at the eastern and south-eastern parts of Krishna and Cauvery basins (represented by the
421 scatter below the regression line till 17° N latitude in Fig. 6.a) due to declining rainfall (Fig. 6c). This considerable
422 variability, on average, reduces the overall contributions of South-West monsoon to annual flow in southern
423 Peninsula with respect to the basins in the northern part.

424 The northern part of the Peninsular region receives comparatively higher rainfall than the southern part without
425 considering the Western Ghats. This increased rainfall is attributed to the movement of low-pressure systems that
426 develop over the Bay of Bengal towards central India (Krishnamurthy & Ajayamohan, 2010; Prakash et al., 2015).
427 The low-pressure systems are a regular feature of South-West monsoon, which brings significant amount of
428 rainfall in the northern part of the Peninsular region (Krishnamurthy & Ajayamohan, 2010). The increased rainfall
429 (Fig. 6.b – after 16° N latitude) is responsible for higher contribution of South-West monsoon flows to annual
430 flow in the northern basins. As the spatial variability of this rainfall is comparatively less than in the southern
431 Peninsular region, there is less variability in the contribution of South-West monsoon flows to annual flow. The
432 spatial variability in South-West monsoon along the south-north direction across Peninsular region can explain
433 the gradient in the contribution of South-West monsoon flows to annual flow in the same direction.

434 On the other hand, the contribution of North-East monsoon flows to annual flow increases in the southerly
435 direction (Fig. 6.d and Fig. 6.e). This can be explained by the fact that the southern part of the Peninsular region
436 receives higher rainfall during North-East monsoon than the rest of the Peninsular region (Fig. 6.f).



437

438 **Figure 6.** Contribution of seasonal flows to annual flow at regional scale. The spatial variability of South-West
 439 and North-East monsoons can explain the variation in contributions of seasonal flows to annual flow across south-
 440 north gradient. The green box in (b) indicates the northern part of peninsular region which receives higher rainfall
 441 than the southern part. The green box in (c) indicates the spatial extent of the rainfall grids which was considered
 442 in figure (b). The red line in figure (b) indicates the mean rainfall – obtained by averaging the rainfall values at a
 443 specific latitude (°N).

444 The application of the analysis framework used here is based on the critical assumption of independence of flows
445 between different seasons (months), which needs to be critically evaluated. Moisture carry-over across seasons is
446 a confounding issue in the case of strongly seasonal catchments (i.e., exhibiting sharp transition from wet season
447 to dry season in terms of rainfall climatology), specifically when the initial wetness condition at the onset of the
448 dry season depends on the final wetness at the end of wet season and vice-versa. Although most of the rainfall
449 (58-90%) is concentrated during South-West monsoon months (i.e., June – September, red bar in Fig. S7) in
450 Peninsular basins, more than 10% of the annual rainfall is received during North-East monsoon months (i.e.,
451 October – December, yellow bar for Cauvery and Krishna in Fig. S7). In addition, more than 8% of annual rainfall
452 occurs in non-monsoon season (i.e., January – May, blue bar in Fig. S7). This highlights that rainfall received
453 during non-monsoon and North-East monsoon seasons are comparable, and thus it is difficult to distinguish the
454 rainfall climatology across these seasons. Therefore, it is challenging to declare these are catchments with
455 seasonally dry climates. In order to justify our assumption in the reconstruction of annual FDC from seasonal
456 flows, we have now conducted a multivariate Hoeffding test (Gaißer et al., 2010) to check the independence
457 between three random variables representing Non-monsoon, South-West Monsoon and North-East Monsoon
458 flows respectively. A value of test statistic – φ^2 – close to zero indicates independence between three random
459 variables. It is observed that except for two stations in Krishna basin, 60 out of 62 stations show independence
460 between flows across the seasons (Fig. S8). This supports appropriateness of the assumption of no carry-over that
461 had been used in this study to construct annual FDC based on seasonal FDCs.

462 **4.2 Combined influence of time scale and process scale partitioning**

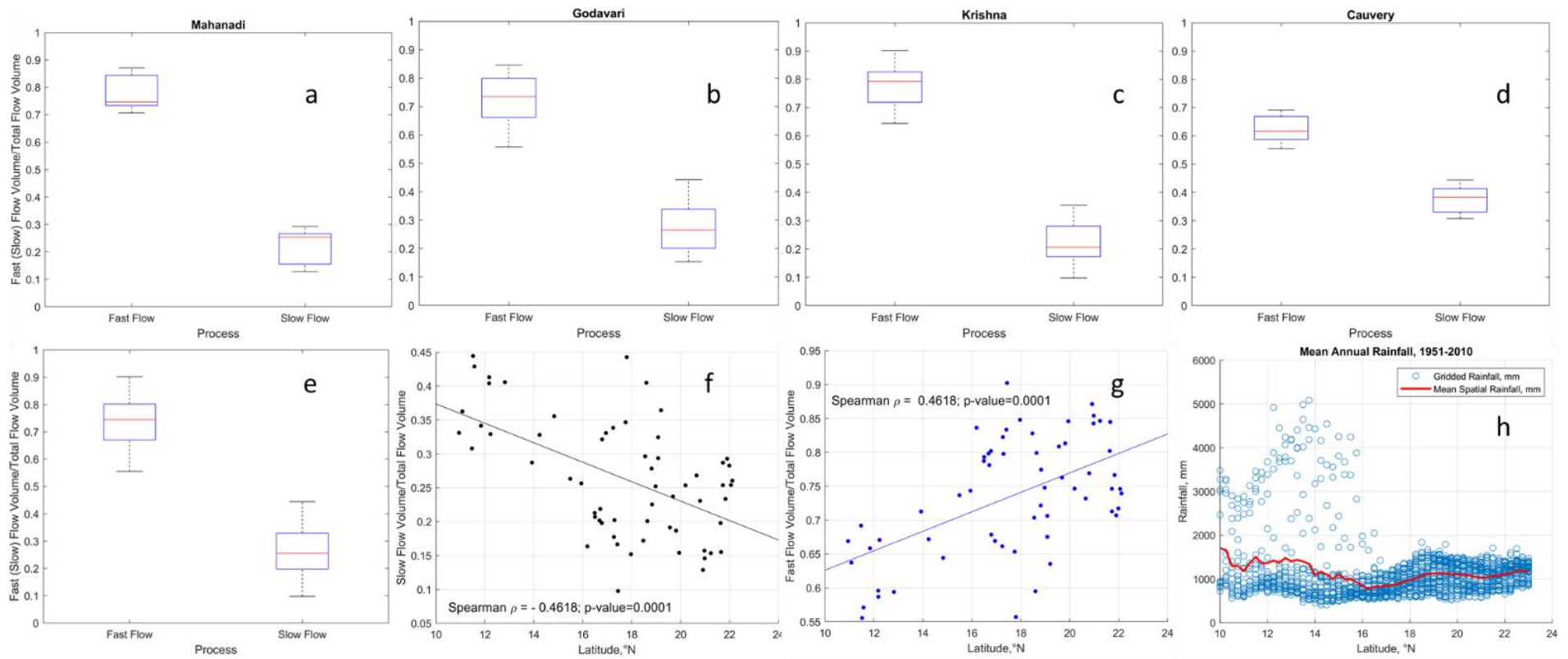
463 In order to further explore the climatic and landscape controls of streamflow variability regionally, we next
464 partition streamflow into fast and slow flow components, notionally representing surface runoff, and a
465 combination of subsurface and groundwater flow respectively (Ghotbi et al., 2020a, b). Fast flow is controlled by
466 event scale runoff generation processes and its variability is characterized by topography, land use, soil and rainfall
467 characteristics. On the other hand, climate seasonality and geologic formations of the subsurface are primary
468 controllers of slow flow variability (Ghotbi et al., 2020a, b). The slow flow component is extracted from observed
469 streamflow by using a recursive digital filter (see details in Text T5 of Supplementary Information). The fast flow
470 component is obtained by then subtracting the slow flow from observed streamflow. The relative contributions of
471 fast flow and slow flow to total flow (and hence also mean annual flow) are estimated using equations 11 and 12
472 respectively, for all the gauging stations across all four basins. The relative contributions of fast and slow flows
473 to total flow at the basin and regional scales (combining all the gauging stations) are shown in Fig. 7. In addition,
474 the long-term mean annual rainfall across the Peninsular region is also presented for comparison and to possibly
475 explain the contributions of fast flow (Fig. 7.h).

476 The contributions of fast and slow flows to total flow in each of the four river basins is presented in Fig. 7.a to
477 Fig. 7.d, indicating a strong dominance of fast flow in the northern basins (close to 80% in Mahanadi, Godavari
478 and Krishna), and relatively less dominance (around 60%) in the southern Cauvery basin. This dominance of fast
479 flow also shows up at the regional scale (Fig. 7.e). The regional variations of the relative contributions of slow
480 and fast flows to total flow can also be seen in the results for individual gauges presented in Fig. 7.f and Fig. 7.g,
481 respectively. On average, the contribution of slow flow decreases in the northerly direction, while the contribution
482 of fast flow increases in a corresponding way.

483 The contribution of fast flow to total flow increases in the northern direction of the Peninsular region (Fig. 7.g).
484 The fast flow component of streamflow is generally more responsive to the characteristics of rainfall intensity.
485 The southern part of the region receives high rainfall over Western Ghats along the western edge of Krishna basin
486 and Cauvery basin (Fig. 7.h). In Cauvery basin, the headwater catchments (namely, MH Halli, Muthankera and
487 Thengumarahada in Fig. S6) contribute 57 – 65 % of fast flow to total flow locally. The subbasins located at the
488 western edges of Krishna basin contribute 80% of the fast flow to total flow (between 13° N and 18°N latitudes
489 in Fig. 7.g) locally. However, there is a wide range of variability in the contributions of fast flow to total flow for
490 subbasins located in the eastern part of Krishna basin. The spatial mean rainfall increases and variability decreases
491 after 16° N latitude (Fig. 7.h), which dictate the increased contribution fast flow to total flow. Therefore, the
492 spatial characteristics (mean and variability) of annual rainfall control the south-north gradient in fast flow
493 contributions to total flow. In order to explain the variability in slow flow fraction of total flow, a multivariate
494 regression analysis is performed (details are provided in Text T8). It is observed that the location of the gauges is
495 an important predictor of the slow flow fraction of total flow in Peninsular region, revealing the existence of
496 regional groundwater gradient in the region (Table T1). In addition to the location of the gauges, the recession
497 parameter, β – that controls the aquifer geometry and water level elevation profile during early and late stages of
498 recession – is found to be significant in explaining the slow flow fraction of total flow (Table T1).

499 The contributions of slow flow to total flow increases in the southerly direction over the Peninsular region (Fig.
500 7.f). This can be explained by two major factors. Firstly, the Peninsular region is mostly dominated by hard rock
501 geologic formations, where the subsurface flows are controlled by secondary porosities due to weathering and
502 fracturing (Chandra, 2018; Das, 2019). The distribution of these formations is highly heterogenous (Fig. 1.c) and
503 is responsible for baseflow (slow flow) contribution to total flow (Collins et al., 2020; Narasimhan, 2006). For
504 example, 84% of the total area of Cauvery basin is classified as moderate and good groundwater potential zone
505 (Arulbalaji et al., 2019). The influence of such potential regions of Cauvery basin is reflected on the presence of
506 significant amount of slow flow even in the Non-monsoon season (Fig. 8.g and Fig. 8.h). Likewise, 63% of the
507 total area of Krishna basin is classified under same category (Harini et al., 2018). However, the slow flow regime
508 becomes much more seasonal (Fig. 8) in the northern part of the Peninsular region due to limited capability of
509 geologic formations in transmitting slow flow (Patil et al., 2017) as well as strong seasonality in rainfall patterns
510 (Fig. 8). Secondly, the southern part of the Peninsula receives rainfall almost equally during both South-West and
511 North-East monsoons, which is reflected in the bimodal pattern of rainfall seasonality (Fig. 8.g and Fig. 8.h). The
512 compounding effect of bimodal rainfall seasonality and higher fraction of moderate to good groundwater potential
513 zones explains the higher contribution of slow flow to total flow in southern part of the Peninsular region.

514

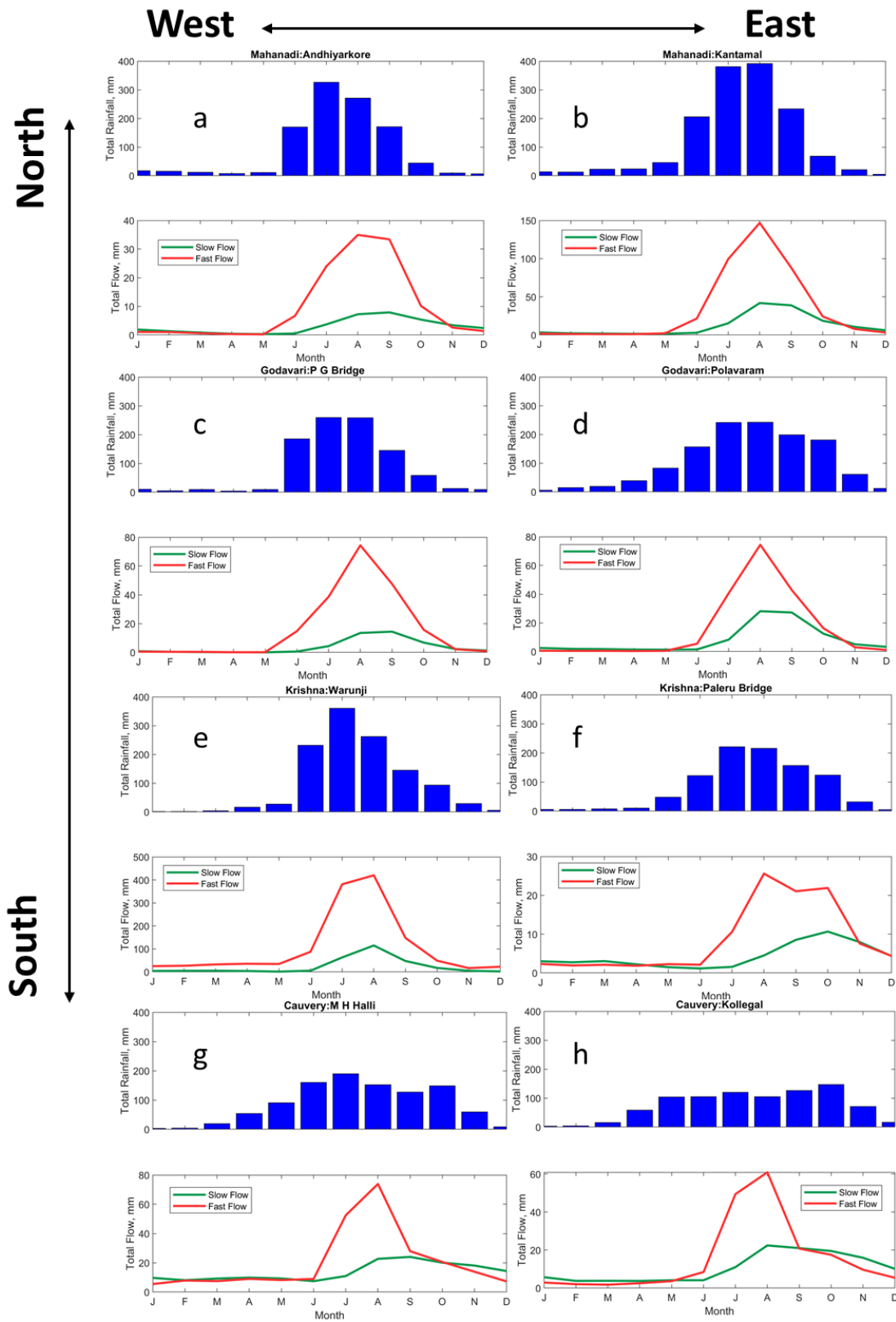


515

516 **Figure 7.** Relative contributions of fast and slow flow to total flow. Consistent higher contribution of fast flow and lower contribution of slow flow to total flow are observed
517 in Peninsular India (a – d) at basin scale. At regional scale, a systematic gradient in fast and slow flow contributions is observed (f and g). The spatial patterns of rainfall (h)
518 can explain the gradient in fast flow contributions. The high scatter of rainfall in the low latitudes represents the heavy rainfall with high variability occurring in the Western
519 Ghats.

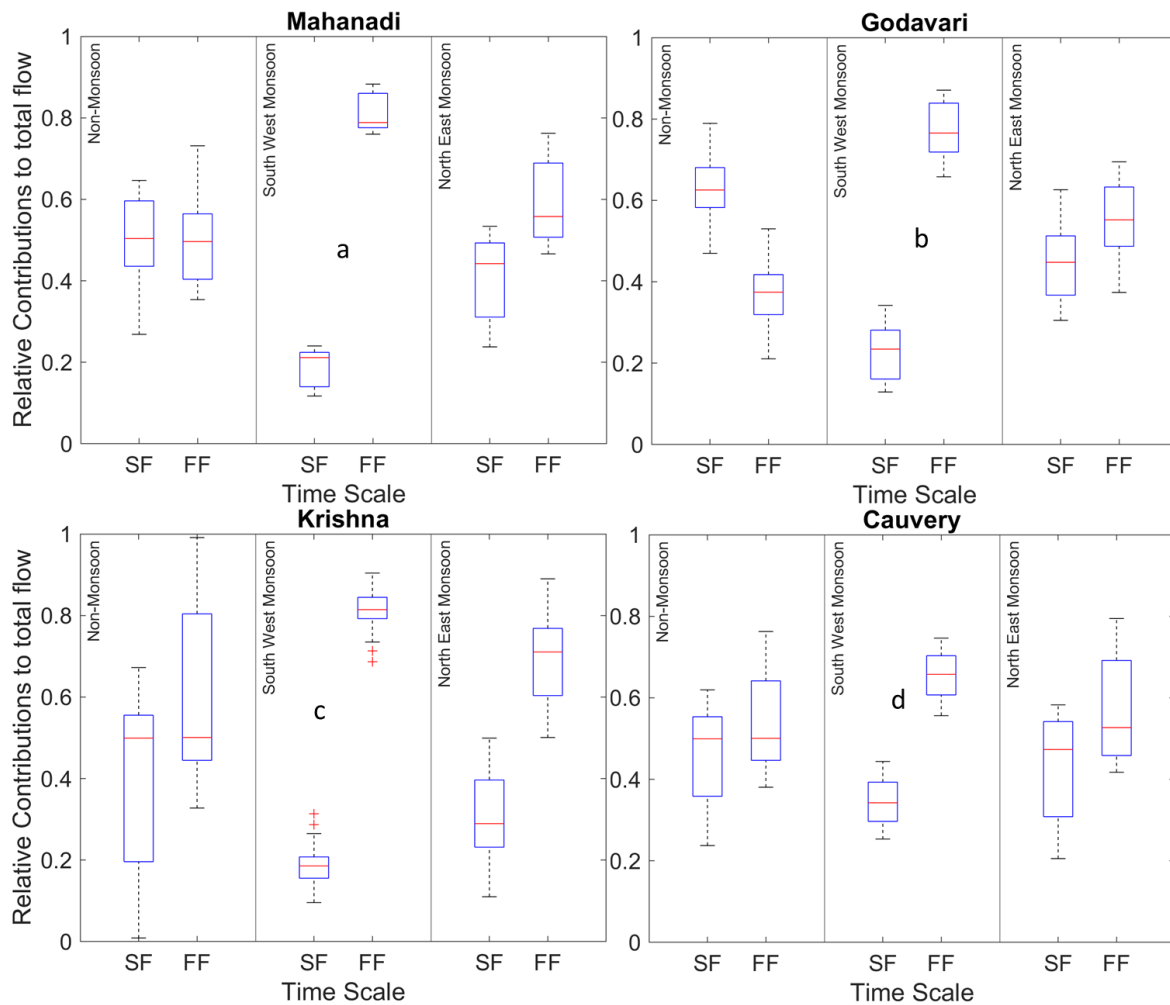
520 Further, an investigation of the combined influence of climatic time scales and process time scales is therefore
521 pertinent to fully understand the controls of streamflow variability in this region. To address this question, we
522 extracted the fast and slow flow components for each of the Non-monsoon, South-West monsoon and North-East
523 monsoon seasons. These components are then used to estimate their relative contributions to total flow for the
524 three seasons across all the gauging stations.

525 The relative contributions of fast and slow flow to total flow at basin scale are shown in Fig. 9. It is observed that
526 during the Non-monsoon period, the median contributions of fast and slow flow for Mahanadi, Krishna and
527 Cauvery basins are similar, although there exists considerable variability in their distribution. With the onset of
528 the South-West monsoon, the contribution of fast flow to total flow increases markedly for all the basins, although
529 relatively much less in the Cauvery basin. During the subsequent North-East monsoon season, the contribution of
530 fast flow decreases whereas slow flow contribution increases. The fluctuations in the fast flow contributions can
531 be explained by the onset and withdrawal of the monsoon seasons, which are major contributors to fast flow
532 generation. The fluctuations in the fast flow contributions across seasons can be explained by the differences in
533 the rainfall amount during South-West and North-East monsoons (Fig. 6.c and Fig. 6.f). Among all four basins,
534 the difference in median contributions of fast and slow flow is minimum. These can be attributed to the presence
535 of higher fraction of moderate and good groundwater potential zones (Arulbalaji et al., 2019) which promotes
536 baseflow even in dry periods (Fig. 8.g and Fig. 8.h). The presence of bimodal pattern in rainfall seasonality due
537 to both South-West and North-East monsoons minimizes the difference between the relative contributions of fast
538 and slow flow to total flow.



539

540 **Figure 8.** Spatial variation of long-term monthly fast and slow flow components of streamflow at selected gauges
 541 in Peninsular region. The blue bar plots represent the long-term monthly rainfall averaged over the sub-basins
 542 corresponding to the gauging stations. The seasonality in rainfall patterns changes (unimodal to bimodal) across
 543 north-south direction of the Peninsular region.



544

545 **Figure 9.** Seasonal contributions of fast (FF) and slow flow (SF) to total flow at basin scale.

546

547 **5. Stratification of streamflow variability**

548 **5.1 Understanding physical controls and spatial variation of flow duration curve by fitting statistical**
 549 **distributions**

550 So far in this paper, in order to understand the physical controls on regional streamflow variability across
 551 Peninsular India we have partitioned observed streamflow in two ways: (i) seasonal/monthly flows, and (ii) slow
 552 and fast flows. We looked at the relative contributions of these components to mean annual streamflow, looked at
 553 how the relative contributions varied regionally, and attributed these to the relative strengths of the monsoons and
 554 spatial variations of geological formations. We now return to the FDCs of the flow components, especially the
 555 shapes of the FDCs (as reflected in the parameters of the fitted distribution) and look at how they themselves vary
 556 regionally.

557 In our study the fast and slow flow time series are scaled by their respective long-term mean values to remove the
 558 influence of mean climate and geology, thus providing an opportunity to identify the secondary controls on the
 559 variation of shapes of FDCs. The scaled fast and slow flow time series are now used to fit the mixed gamma
 560 distribution (MGD, (see details in Text T4 of Supplementary Information). The parameters of mixed gamma

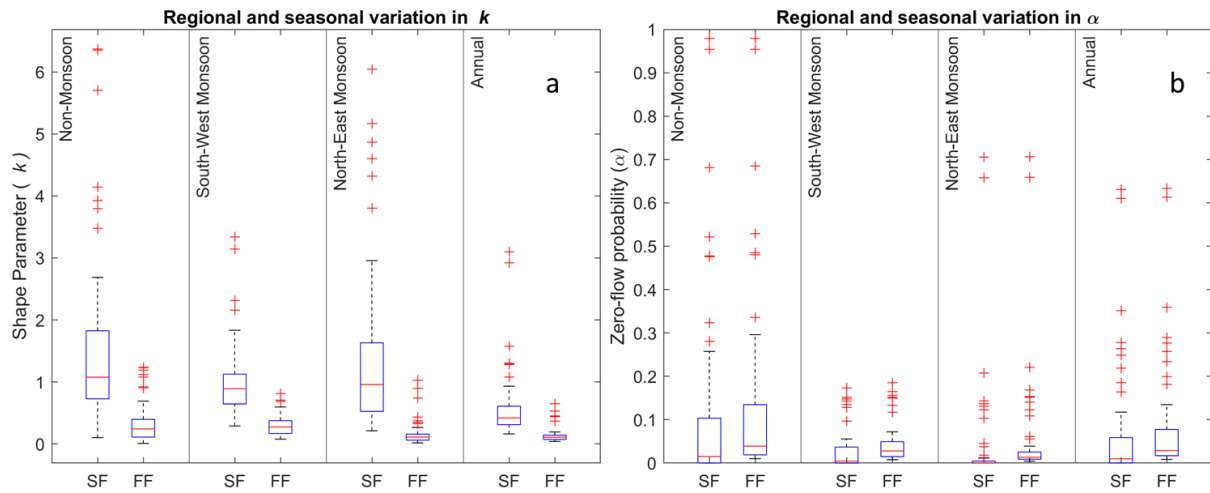
561 distribution control the shape and orientation of the FDC. For example, the shape parameter k controls the slope
562 of the FDC whereas α controls the zero-flow part of the FDC. However, the parameter θ affects the vertical shift
563 of the FDC. In addition, these parameters are also linked with the mean and variance of the streamflow time series.
564 For example, the scale parameter θ is directly proportional to the mean of the time series whereas, the shape
565 parameter k is inversely proportional to the variance of the time series.

566 As the fast and slow flow time series are scaled with their respective long-term means, the scale parameter (θ) is
567 approximately found to be inversely proportional to shape parameter (k) through the relationship, $k\theta = \frac{1}{1-\alpha}$
568 (Cheng et al., 2012). Therefore, the variations of only k and α – zero-flow probability, are presented in this section.
569 The variation of k can be related to the steepness of the FDC, i.e., smaller values of k will have steeper slopes.

570 The Nash-Sutcliffe efficiency (NSE) and coefficient of determination (R^2) goodness of fit of fast/slow flows to
571 MGD is shown in Fig. S10 (in Supplementary Information). In addition, the observed and simulated fast and slow
572 flow FDCs are compared in Fig. S8 (in Supplementary Information). It is observed that the slow flow component
573 fits well to mixed gamma distribution than fast flow component, as slow flow is most stable component and MGD
574 satisfactorily captured the shape of slow flow FDC. However, MGD adequately captures the shape of fast flow
575 FDCs at upper tail (high flow segment), except for the lower tail (low flow segment). The fast flow processes are
576 governed by more complex processes (for example, infiltration and saturation excess runoff generation, runoff
577 routing, stochastic nature of storm events, properties of soil and topography etc.) than slow flow (for example,
578 climate seasonality and underlying geology of aquifer system).

579 The seasonal variation of parameters of the mixed gamma distribution at regional scale (comprising of all the
580 gauging stations) is presented in Fig. 10. The mixed gamma distribution performed well in fitting the flow duration
581 curves of two flow components across different seasons (Fig. S10). In Fig. 10.a, it is observed that the shape
582 parameter of slow flow is consistently higher than that of fast flow. The shape parameter is inversely proportional
583 to the variance of streamflow. The slow flow exhibits lower variance due to its longer time of residence in the
584 subsurface formations. Moreover, the subsurface formations in Cauvery River basin are more favourable to slow
585 flow in comparison to the other three basins (Fig. 8.g and Fig. 8.h). In addition, the bimodal seasonal pattern of
586 rainfall is also responsible for occurrence of slow flow even in the Non-monsoon period for the southern basins
587 (Fig. 8).

588 The fast flow component exhibits higher variance than the slow flow component. The median shape parameter of
589 fast flow is highest during South-West monsoon season and lowest during North-East monsoon (Fig. 10.a). This
590 can be explained by the lower variance of fast flow during South-West monsoon as the rainfall amount is higher
591 during the season compared to the North-East monsoon (Fig. 6.c and Fig. 6.f). The dominance of both South-
592 West and North-East monsoons in Cauvery basin results in lower variance of fast flow compared to the northern
593 basins. The fast flow duration curves are steeper than the slow flow duration curves for all seasons, as the
594 magnitudes of k for fast flow are smaller than that of slow flow (Fig. 10.a).



595

596 **Figure 10.** Regional and seasonal variation of k and α parameter of mixed gamma distribution.

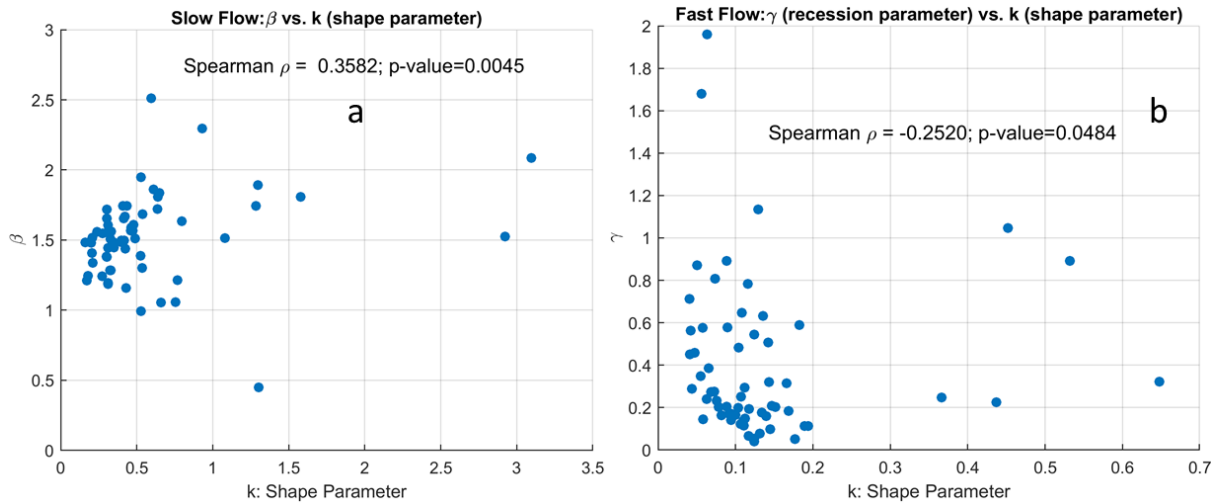
597 The parameter α controls the zero-flow part of the flow duration curve. It is observed that the mean α for slow
 598 flow is minimum during South-West monsoon and maximum for Non-monsoon season (Fig. 10.b) on a regional
 599 scale. This can be attributed to the combined influence of rainfall during South-West monsoon and the
 600 connectivity between underlying geologic formations in the Peninsular region. For the fast flow, the mean α is
 601 minimum during the South-West monsoon and maximum during Non-monsoon as the South-West monsoon is
 602 the dominating rainfall season in Peninsular India.

603 The shape parameters (k) of MGD for slow and fast flow components are linked with landscape properties through
 604 recession analysis, where the parameters γ and β of power-law relationship are estimated using streamflow data
 605 (details in Text T6 in Supplementary Information). It is observed that shape parameter (inversely proportional to
 606 variability) of slow flow is positively correlated with β . The parameter β is influenced by aquifer geometry and
 607 water table elevation profile defining early and late stages of recession (Tashie et al., 2020a; Tashie et al., 2020b).
 608 Higher values of β indicate slow late recessions which is characterized by low variability in slow flow (Fig. 11.a).

609 The shape parameter of fast flow is negatively correlated with the parameter γ of the power-law relationship (Fig.
 610 11.b). The parameter γ strongly related with the seasonality of catchment wetness and evapotranspiration which
 611 are primary governing factors for runoff generation (Dralle et al., 2015; Gnann et al., 2021). In addition, the spatial
 612 variation of rainfall also influences the variability of γ (Biswal & Kumar, 2014) which reflects the variability of
 613 fast flow.

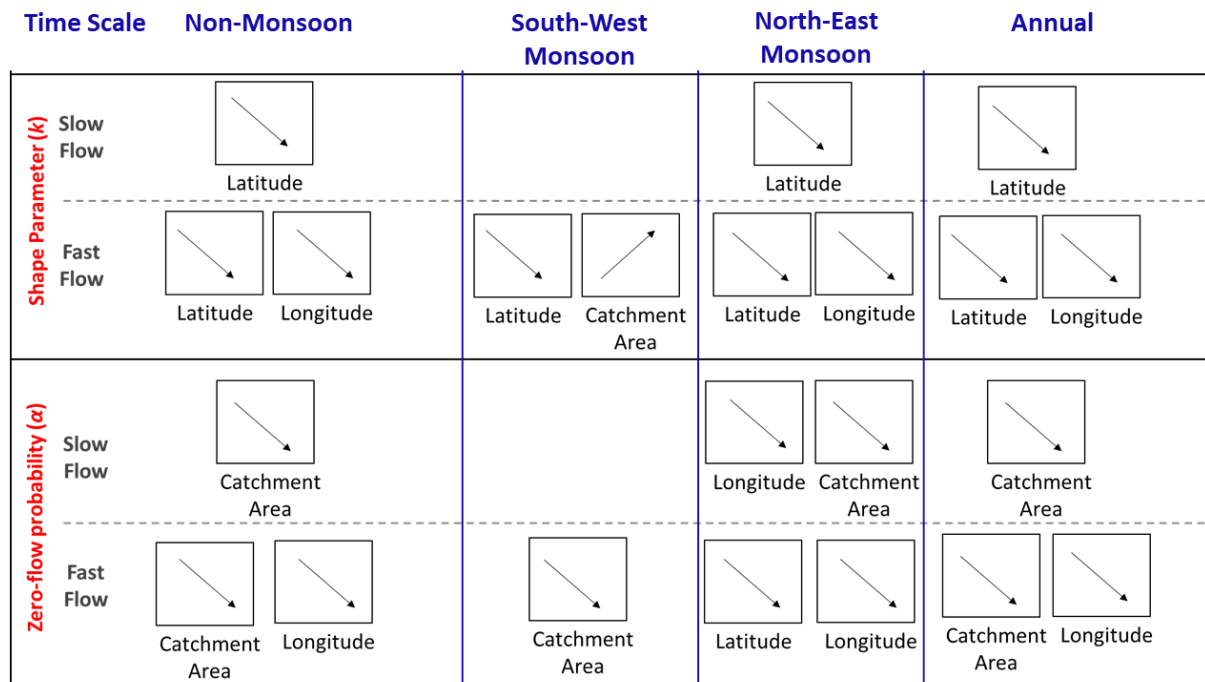
614 The variation of the parameters, k and α was also studied using spatial descriptors (latitude and longitude) as
 615 explanatory variables to understand the spatial variation of FDCs across south-north, west-east gradients. In
 616 addition, the behaviour of these parameters is also assessed using catchment area as another explanatory variable.
 617 The regional parameter sets comprising of k and α are next constructed for slow and fast flow processes by
 618 including these parameters for all the time series across different gauging stations across the Peninsular region.
 619 The Spearman correlation coefficients between these parameters and explanatory variables (i.e., catchment area
 620 and spatial descriptors – latitude and longitude) for slow and fast flow processes at seasonal scales are computed.

621 The schematic representation of significant directions (positive/negative correlations) in Spearman coefficient is
 622 shown in Fig. 12.



623

624 **Figure 11.** Relationship between flow variability (related inversely to shape parameter, k of mixed gamma
 625 distribution) and recession parameters.



626

627 **Figure 12.** Schematic representation of spatial and temporal variation of parameters of mixed gamma distribution
 628 across Peninsular India. The direction of significant Spearman correlation coefficient between model parameters
 629 and descriptors (catchment area and spatial descriptors – latitude and longitude) for fast and slow flow across
 630 multiple time scale is presented.

631 The shape parameter of fast flow is found to be positively correlated with catchment area (Fig. 12, top panel),
 632 implying lower variability of fast flow in large catchments. This can be attributed to increased smoothing effect
 633 of incoming rainfall in larger catchments through various storages, thus reducing the variability of fast flow.
 634 Moreover, the shape parameters for fast flow are negatively correlated with spatial descriptors, indicating

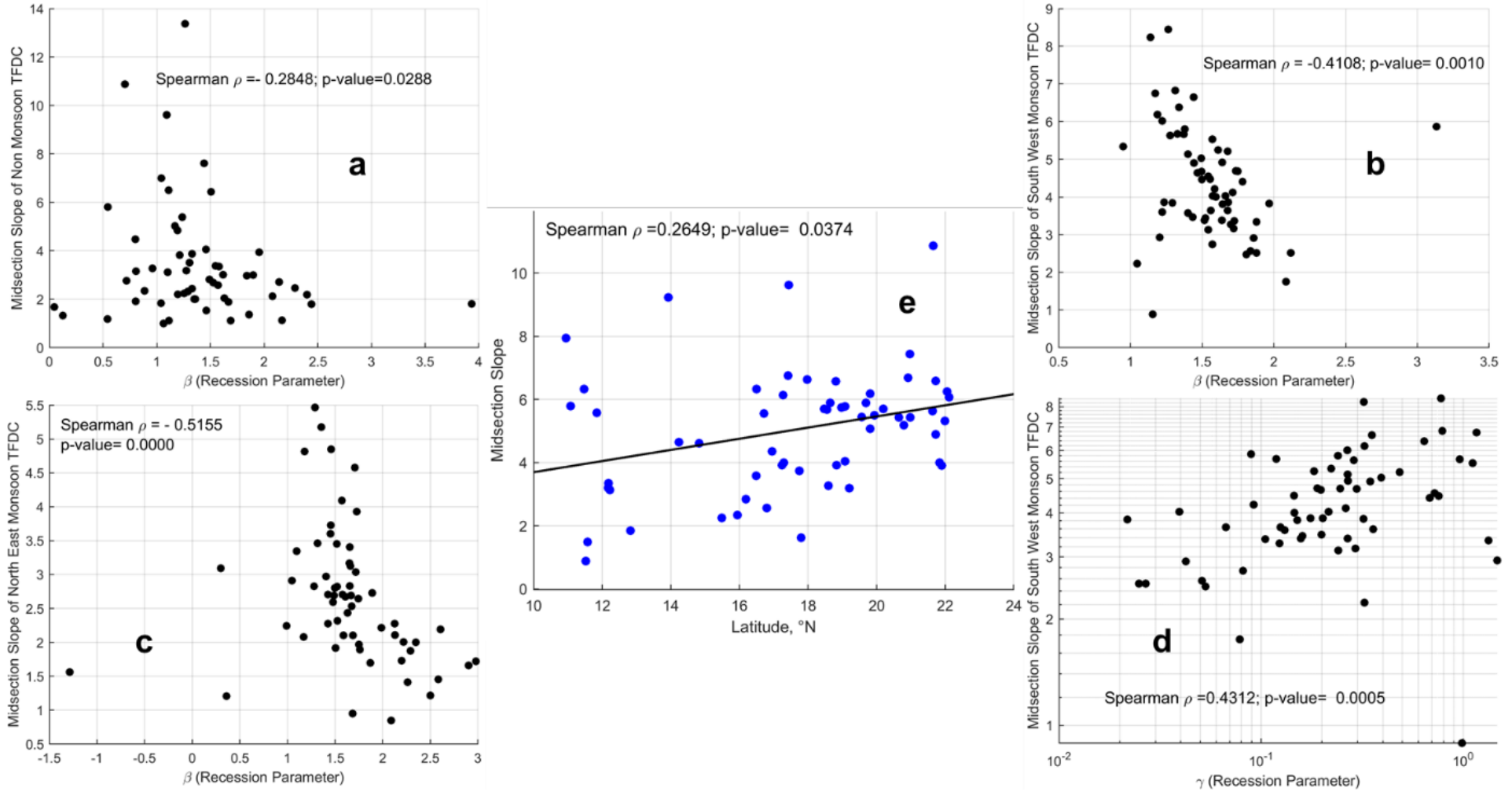
635 increased variability of fast flow along south-north and west-east gradients. This can be partly explained by the
636 bimodal seasonal pattern of rainfall due to dominance of South-West and North-East monsoons, thus reducing the
637 variability of fast flow in the southern part of the region. The rainfall pattern becomes more seasonal (primarily
638 due to South-West monsoon) in the northern part of region which can contribute to increased variability of fast
639 flow. The presence of numerous water retention structures for supporting irrigation in these regions (54 – 75% of
640 Peninsular basins are crop land) can modify the variability of the flow, although we have not analysed this
641 separately in this study.

642 The shape parameter of slow flow is found to be negatively correlated with latitude, implying that slow flow
643 becomes highly variable in the northern part of the region. This can be explained by the nature of geologic
644 formations in the Cauvery basin that promotes slow flow even during the Non-monsoon period. However, in the
645 northern part of the region, the slow flow tends to become more seasonal and has very limited flow during non-
646 rainy seasons. In addition to the geology, the bimodal seasonal rainfall patterns due to monsoons can play an
647 important role in the variability of slow flow. Apart from the spatial descriptors, the slow flow variability is
648 inversely proportional to catchment area, implying larger catchments have lower slow flow variability than
649 smaller catchments. This can be explained by the proportional increase in area of contribution to slow flow with
650 increase in catchment size, thus reducing the variability in slow flow for larger catchments.

651 The parameter α is found to be negatively correlated with catchment area (Fig. 12, bottom panel) for fast and slow
652 processes, implying zero-flow probabilities are lower for larger catchments. The higher residence time of water
653 in larger catchment due to various kinds of storages facilitates flow in river even in Non-monsoon season, thus
654 reducing the zero-flow probabilities. In addition, the parameter α of both slow and fast flow are negatively
655 correlated with longitude, implying lower zero-flow probabilities along west-east direction. This can be attributed
656 to natural declining elevation (Fig. S1.b) which promotes both fast and slow flow towards eastern direction.

657 **5.2 Understanding physical controls and spatial variation of seasonal flow duration curve using mid-section** 658 **slope**

659 Apart from mean, variance and no-flow frequency, the midsection slope of the FDC – estimated using
660 $\frac{\ln(Q_{33p}) - \ln(Q_{66p})}{0.66 - 0.33}$, where Q_{33p} and Q_{66p} represent the streamflow values at 33rd and 66th percentiles respectively –
661 is connected to the average flow regime of the catchment, which is controlled by both surface and subsurface
662 processes (Yokoo & Sivapalan, 2011; Chouaib et al., 2018). The association of the slope of FDC with the
663 parameters pertaining to recession analysis is presented in Fig. 13.



666 **Figure 13.** Association between streamflow variability and recession parameters.

667 During Non-monsoon and North East monsoon seasons (Fig. 13a and Fig. 13c) – when rainfall is comparatively
668 less than South West monsoon – a significant association between flow variability and β highlights the importance
669 of slow flow and recession characteristics controlled by aquifer geometry and water table elevation profile. In
670 addition to significant association with β during South West monsoon (Fig. 13b), the midsection slope of FDC is
671 positively correlated with γ – the parameter which is strongly related with the seasonality of catchment wetness,
672 evapotranspiration and spatial variation in rainfall – revealing the importance of land surface processes in
673 variability of streamflow variability.

674 A coherent pattern in variability of streamflow (via. Midsection slope of FDC) is observed across South – North
675 gradient of the Peninsular region (Fig. 13e). This systematic pattern in streamflow variability reflects the influence
676 of combined functioning of subsurface and land surface processes on regional hydrologic signatures of Peninsular
677 India.

678 **6. Conclusions**

679 The comprehensive analysis of spatial variations in seasonal and annual flow duration curves across Peninsular
680 India has provided valuable insights into the controls of streamflow variability at different scales. The partitioning
681 framework employed in this study effectively approximated annual flow duration curves, confirming its efficacy
682 in capturing the intricate dynamics of seasonal and monthly flows. Noteworthy spatial patterns emerged, with
683 gauging stations in the northern part of the peninsula exhibiting higher dominance of South-West monsoon flows
684 in contrast to the more balanced contributions observed in the southern regions, where North-East monsoon flows
685 also played a significant role.

686 The regional-scale analysis unveiled the influence of spatial patterns of monsoon rainfall, showing increased
687 contributions of South-West monsoon flows in the northerly direction and elevated contributions of North-East
688 monsoon flows in the southerly direction. The study also delved into the partitioning of streamflow into fast and
689 slow components, revealing a dominance of fast flow in northern basins and an increasing contribution of slow
690 flow in the southerly direction. Factors such as rainfall intensity, geologic formations, and groundwater gradients
691 were identified as critical controls shaping these flow characteristics. The investigation of combined influences
692 of climatic time scales and process time scales further enriched our understanding of streamflow variability.
693 Seasonal fluctuations in fast and slow flow contributions highlighted the dynamic nature of streamflow response
694 to monsoon onset and withdrawal. The study emphasized the importance of considering both climatic and
695 landscape factors across different scales to comprehensively grasp the controls of streamflow variability in the
696 Peninsular region.

697 By undertaking an extensive analysis of flow duration curves for both fast and slow flow components across
698 different seasons, the study aims to understand the variations and controls governing these hydrological patterns.
699 The initial step of scaling the fast and slow flow time series by their respective long-term mean values serves as
700 a crucial tool in isolating secondary controls on FDC shapes, effectively removing the influence of mean climate
701 and geology. The subsequent use of the Mixed Gamma Distribution to fit the scaled time series allows for an
702 advanced examination of the parameters influencing FDC shapes, with a focus on the key factors of shape
703 parameter (k) and probability of zero flows (α). The seasonal variations of MGD parameters at a regional scale

704 reveal the impact of monsoons on streamflow characteristics. Notably, the consistently higher shape parameters
705 for slow flow highlight the lower variance attributed to longer residence times in subsurface formations,
706 emphasizing the influence of geological features.

707 Further exploration into the relationships between MGD parameters and landscape properties through recession
708 analysis enhances our understanding of hydrological controls. The positive correlation between the shape
709 parameter of slow flow and recession parameter β , influenced by aquifer geometry, contrasts with the negative
710 correlation between the shape parameter of fast flow and the parameter γ , associated with seasonality of catchment
711 wetness and evapotranspiration. Spatial variation analysis using descriptors like latitude, longitude, and catchment
712 area unveils significant correlations, offering insights into the influence of geographical factors on FDC shapes.
713 The correlation of fast flow shape parameters with catchment area suggests reduced variability in larger
714 catchments, while the negative correlation of slow flow shape parameters with latitude indicates increased
715 variability in the northern part of the region. The examination of zero-flow probabilities controlled by the
716 parameter α reveals noteworthy trends. Larger catchments exhibit lower zero-flow probabilities, and the negative
717 correlation of α with longitude highlights the spatial influence along the west-east direction. Finally, the study
718 explores the midsection slope of the FDC, connecting it to average flow regimes controlled by both surface and
719 subsurface processes. Associations with recession analysis parameters underline the integrated influence of
720 aquifer geometry and land surface processes on streamflow variability across Peninsular India.

721 In summary, the methodology employed in this study offers a systematic and insightful approach to unravelling
722 the complexities of streamflow variability across Peninsular India. This study not only enhances our understanding
723 of the relative contributions and shapes of FDCs but also sheds light on the intricate interplay of geological,
724 spatial, and hydrological factors influencing streamflow variability in this region.

725 We acknowledge, however, that in recent times streamflow variability in Peninsular India has been significantly
726 impacted by anthropogenic activities, including significant land use and land cover changes, and other human
727 interferences such as the building of dams and the extraction of water from both rivers and from groundwater
728 aquifers for human use. The present study has not explored the effects of human impacts: their impacts on both
729 temporal (inter-decadal) and spatial (regional) variations of the FDCs is left for future work. Further work is also
730 needed to understand in more detail the causes and the relative contributions of regional patterns precipitation and
731 geological formations on streamflow partitioning.

732 On the methodological front, there is opportunity to refine the analysis used here to incorporate the statistical
733 cross-correlation between fast and slow flows in the reconstruction of the FDC for total streamflow, by adopting
734 generalized approaches (e.g., copulas). In the exploration of the relative contributions of the monsoons, there is
735 scope to extend the analysis framework to partition the streamflow variability guided by the actual breakdown
736 into the seasons each year in a more flexible way, as opposed to the static way. This is likely to make the results
737 of the analysis more robust and less uncertain. Finally, in the process domain, the filter-based separation of total
738 streamflow into fast and slow flow can be variably impacted by catchment size, introducing some uncertainty into
739 the partitioning of the FDC of total streamflow into its fast flow and slow flow components. Future work in this
740 area should explore ways to overcome these methodological shortcomings.

741

742 *Data availability.* The streamflow datasets used for the analysis are accessible from
743 <https://indiawris.gov.in/wris/#/>. The daily India Meteorological Department (IMD) gridded rainfall product at
744 spatial resolution of $0.25^\circ \times 0.25^\circ$
745 (https://www.imdpune.gov.in/Clim_Pred_LRF_New/Grided_Data_Download.html) from Pai et al., (2014) is
746 used. The function baseflow, used for partitioning total flow to slow flow is downloaded from
747 [https://in.mathworks.com/matlabcentral/fileexchange/58525-baseflow-filter-using-the-recursive-digital-filter-](https://in.mathworks.com/matlabcentral/fileexchange/58525-baseflow-filter-using-the-recursive-digital-filter-technique)
748 [technique](https://in.mathworks.com/matlabcentral/fileexchange/58525-baseflow-filter-using-the-recursive-digital-filter-technique).

749 *Author contributions.* PD, JM, and MS conceptualized the work, developed the methodology, and carried out the
750 data curation, formal analysis, validation, and writing of the original draft. MS and PPM reviewed the initial
751 manuscript, and PPM provided the resources needed for this work.

752 *Competing interests.* The authors declare that they have no conflict of interest.

753 *Acknowledgements.* PD acknowledges DST INSPIRE Faculty Fellowship (DST/INSPIRE/04/2022/001952
754 Faculty Reference No.: IFA22-EAS 114) received from Department of Science and Technology, Government of
755 India, in Earth and Atmospheric Sciences Division of 2022 call. MS acknowledges the award of a Satish Dhawan
756 Endowed Visiting Professorship that enabled him to visit the Interdisciplinary Centre for Water Research
757 (ICWaR) at the Indian Institute of Science, which allowed him to participate in the research activity that
758 culminated in this paper. MS also acknowledges the generous support and facilities provided by ICWaR that made
759 his stay a very productive one.

760

761 **References**

762 Arai, R., Toyoda, Y., & Kazama, S. (2021). Runoff recession features in an analytical probabilistic streamflow
763 model. *Journal of Hydrology*, 597, 125745.

764 Arulbalaji, P., Sreelash, K., Maya, K., and Padmalal, D.: Hydrological assessment of groundwater potential zones
765 of Cauvery River Basin, India: a geospatial approach, *Environ. Earth Sci.*, 78, 1–21,
766 <https://doi.org/10.1007/s12665-019-8673-6>, 2019.

767 Basso, S. and Botter, G.: Streamflow variability and optimal capacity of run-of-river hydropower plants, *Water*
768 *Resour. Res.*, 48, 1–13, <https://doi.org/10.1029/2012WR012017>, 2012.

769 Basso, S., Schirmer, M., & Botter, G. (2015). On the emergence of heavy-tailed streamflow distributions.
770 *Advances in Water Resources*, 82, 98-105.

771 Biswal, B. and Nagesh Kumar, D.: Study of dynamic behaviour of recession curves, *Hydrol. Process.*, 28, 784–
772 792, <https://doi.org/10.1002/hyp.9604>, 2014.

773 Blum, A. G., Archfield, S. A., Vogel, R. M., and Survey, G.: On the probability distribution of daily streamflow
774 in the United States, *Hydrol. Earth Syst. Sci.*, 21, 3093–3103, [https://doi.org/https://doi.org/10.5194/hess-21-](https://doi.org/https://doi.org/10.5194/hess-21-3093-2017)
775 [3093-2017](https://doi.org/https://doi.org/10.5194/hess-21-3093-2017), 2017.

776 Botter, G., Zanardo, S., Porporato, A., Rodriguez-Iturbe, I., and Rinaldo, A.: Ecohydrological model of flow
777 duration curves and annual minima, *Water Resour. Res.*, 44, 1–12, <https://doi.org/10.1029/2008WR006814>, 2008.

778 Botter, G., Basso, S., Rodriguez-Iturbe, I., & Rinaldo, A. (2013). Resilience of river flow regimes. *Proceedings*
779 *of the National Academy of Sciences*, 110(32), 12925-12930.

780 Carlier, C., Wirth, S. B., Cochand, F., Hunkeler, D., & Brunner, P. (2018). Geology controls streamflow dynamics.
781 *Journal of Hydrology*, 566, 756-769.

782 Chandra, P. C.: Groundwater of Hard Rock Aquifers of India, 61–84, [https://doi.org/10.1007/978-981-10-3889-](https://doi.org/10.1007/978-981-10-3889-1_5)
783 [1_5](https://doi.org/10.1007/978-981-10-3889-1_5), 2018.

784 Chatterjee, S., Scotese, C. R., and Bajpai, S.: The Restless Indian plate and its epic voyage from Gondwana to
785 Asia: Its tectonic, paleoclimatic, and paleobiogeographic evolution, *Spec. Pap. Geol. Soc. Am.*, 529, 1–147,
786 <https://doi.org/10.1130/2017.2529>, 2017.

787 Cheng, L., Yaeger, M., Viglione, A., Coopersmith, E., Ye, S., and Sivapalan, M.: Exploring the physical controls

- 788 of regional patterns of flow duration curves – Part 1: Insights from statistical analyses, *Hydrol. Earth Syst.*
789 *Sci.*, 16, 4435–4446, <https://doi.org/10.5194/hess-16-4435-2012>, 2012.
- 790 Chouaib, W., Caldwell, P. V., and Alila, Y.: Regional variation of flow duration curves in the eastern United
791 States: Process-based analyses of the interaction between climate and landscape properties, *J. Hydrol.*, 559, 327–
792 346, <https://doi.org/10.1016/j.jhydrol.2018.01.037>, 2018.
- 793 Collins, L. S., Loveless, S. E., Muddu, S., Buvaneshwari, S., Palamakumbura, R. N., Krabbendam, M., Lapworth,
794 D. J., Jackson, C. R., Gooddy, D. C., Nara, S. N. V., Chattopadhyay, S., and MacDonald, A. M.: Groundwater
795 connectivity of a sheared gneiss aquifer in the Cauvery River basin, India, *Hydrogeol. J.*, 28, 1371–1388,
796 <https://doi.org/10.1007/s10040-020-02140-y>, 2020.
- 797 Costa, V. and Fernandes, W.: Regional Modeling of Long-Term and Annual Flow Duration Curves: Reliability
798 for Information Transfer with Evolutionary Polynomial Regression, *J. Hydrol. Eng.*, 26, 1–12,
799 [https://doi.org/10.1061/\(asce\)he.1943-5584.0002051](https://doi.org/10.1061/(asce)he.1943-5584.0002051), 2021.
- 800 Das, S.: Frontiers of Hard Rock Hydrogeology in India, in: *Ground Water Development - Issues and Sustainable*
801 *Solutions*, Springer Singapore, Singapore, 35–68, https://doi.org/10.1007/978-981-13-1771-2_3, 2019.
- 802 Deshpande, N. R., Kothawale, D. R., and Kulkarni, A.: Changes in climate extremes over major river basins of
803 India, *Int. J. Climatol.*, 36, 4548–4559, <https://doi.org/10.1002/joc.4651>, 2016.
- 804 Dralle, D., Karst, N., and Thompson, S. E.: a, b careful: The challenge of scale invariance for comparative analyses
805 in power law models of the streamflow recession, *Geophys. Res. Lett.*, 42, 9285–9293,
806 <https://doi.org/10.1002/2015GL066007>, 2015.
- 807 Durighetto, N., Mariotto, V., Zanetti, F., McGuire, K. J., Mendicino, G., Senatore, A., & Botter, G. (2022).
808 Probabilistic description of streamflow and active length regimes in rivers. *Water Resources Research*, 58,
809 e2021WR031344. <https://doi.org/10.1029/2021WR031344>
- 810 Gadgil, S.: The Indian Monsoon and Its Variability, *Annu. Rev. Earth Planet. Sci.*, 31, 429–467,
811 <https://doi.org/10.1146/annurev.earth.31.100901.141251>, 2003.
- 812 Fenicia, F., Kavetski, D., Savenije, H. H., Clark, M. P., Schoups, G., Pfister, L., & Freer, J. (2014). Catchment
813 properties, function, and conceptual model representation: is there a correspondence? *Hydrological Processes*,
814 28(4), 2451–2467.
- 815 Ghotbi, S., Wang, D., Singh, A., Blöschl, G., and Sivapalan, M.: A New Framework for Exploring Process
816 Controls of Flow Duration Curves, *Water Resour. Res.*, 56, <https://doi.org/10.1029/2019WR026083>, 2020a.
- 817 Ghotbi, S., Wang, D., Singh, A., Mayo, T., and Sivapalan, M.: Climate and Landscape Controls of Regional
818 Patterns of Flow Duration Curves Across the Continental United States: Statistical Approach, *Water Resour. Res.*,
819 56, <https://doi.org/10.1029/2020WR028041>, 2020b.
- 820 Gnann, S. J., McMillan, H. K., Woods, R. A., and Howden, N. J. K.: Including Regional Knowledge Improves
821 Baseflow Signature Predictions in Large Sample Hydrology, *Water Resour. Res.*, 57,
822 <https://doi.org/10.1029/2020WR028354>, 2021.
- 823 Harini, P., Sahadevan, D. K., Das, I. C., Manikyamba, C., Durgaprasad, M., and Nandan, M. J.: Regional
824 Groundwater Assessment of Krishna River Basin Using Integrated GIS Approach, *J. Indian Soc. Remote Sens.*,
825 46, 1365–1377, <https://doi.org/10.1007/s12524-018-0780-4>, 2018.
- 826 Harman, C. and Troch, P. A.: What makes Darwinian hydrology “Darwinian”? Asking a different kind of question
827 about landscapes, *Hydrol. Earth Syst. Sci.*, 18, 417–433, <https://doi.org/10.5194/hess-18-417-2014>, 2014.
- 828 Kale, V. S., Hire, P., and Baker, V. R.: Flood Hydrology and Geomorphology of Monsoon-dominated Rivers:
829 The Indian Peninsula, *Water Int.*, 22, 259–265, <https://doi.org/10.1080/02508069708686717>, 1997.
- 830 Kale, V. S., Vaidyanadhan, R.: *Landscapes and Landforms of India*, edited by: Kale, V. S., Springer Netherlands,
831 Dordrecht, 105–113 pp., https://doi.org/10.1007/978-94-017-8029-2_6, 2014.
- 832 Krishnamurthy, V. and Ajayamohan, R. S.: Composite Structure of Monsoon Low Pressure Systems and Its
833 Relation to Indian Rainfall, *J. Clim.*, 23, 4285–4305, <https://doi.org/10.1175/2010JCLI2953.1>, 2010.
- 834 Krasovskaia, I., Gottschalk, L., Leblois, E., & Pacheco, A. (2006). Regionalization of flow duration curves.
835 *Climate variability and change: hydrological impacts*, 105–110.

836 Leong, C., & Yokoo, Y. (2019). An interpretation of the relationship between dominant rainfall-runoff processes
837 and the shape of flow duration curve by using data-based modeling approach. *Hydrological Research Letters*,
838 13(4), 62-68.

839 Leong, C., & Yokoo, Y. (2022). A multiple hydrograph separation technique for identifying
840 hydrological model structures and an interpretation of dominant process controls on flow
841 duration curves. *Hydrological Processes*, 36(4), e14569. <https://doi.org/10.1002/hyp.14569>

842 Magilligan, F. J. and Nislow, K. H.: Changes in hydrologic regime by dams, *Geomorphology*, 71, 61–78,
843 <https://doi.org/10.1016/j.geomorph.2004.08.017>, 2005.

844 Magilligan, F. J., Nislow, K. H., and Graber, B. E.: Scale-independent assessment of discharge reduction and
845 riparian disconnectivity following flow regulation by dams, *Geology*, 31, 569, [https://doi.org/10.1130/0091-7613\(2003\)031<0569:SAODRA>2.0.CO;2](https://doi.org/10.1130/0091-7613(2003)031<0569:SAODRA>2.0.CO;2), 2003.

847 Müller, M. F., & Thompson, S. E. (2016). Comparing statistical and process-based flow duration curve models in
848 ungauged basins and changing rain regimes. *Hydrology and Earth System Sciences*, 20(2), 669-683.

849 Narasimhan, T. N.: Ground Water in Hard-Rock Areas of Peninsular India: Challenges of Utilization, *Ground*
850 *Water*, 44, 130–133, <https://doi.org/10.1111/j.1745-6584.2005.00167.x>, 2006.

851 Pai, D. S., Sridhar, L., Rajeevan, M., Sreejith, O. P., Satbhai, N. S., and Mukhopadhyay, B.: Development of a
852 new high spatial resolution (0.25° × 0.25°) long period (1901-2010) daily gridded rainfall data set over India and
853 its comparison with existing data sets over the region, *Mausam*, 1, 1–18, 2014.

854 Patil, S., Kulkarni, H., Bhave, N., Development, W. R., Forum, P., Dialogue, P., and Conflicts, W.: Groundwater
855 in the Mahanadi River Basin, <https://doi.org/10.13140/RG.2.2.11561.95846>, 2017.

856 Prakash, S., Mitra, A. K., and Pai, D. S.: Comparing two high-resolution gauge-adjusted multisatellite rainfall
857 products over India for the southwest monsoon period, *Meteorol. Appl.*, 22, 679–688,
858 <https://doi.org/10.1002/met.1502>, 2015.

859 Rajeevan, M., Unnikrishnan, C. K., Bhate, J., Niranjana Kumar, K., and Sreekala, P. P.: Northeast monsoon over
860 India: variability and prediction, *Meteorol. Appl.*, 19, 226–236, <https://doi.org/10.1002/met.1322>, 2012.

861 Ramachandra, T. V: Global Biodiversity Hotspot - Western Ghats : Water Tower of Peninsular India and Precious
862 Heritage for Posterity, 2018.

863 Rehana, S. and Mujumdar, P. P.: River water quality response under hypothetical climate change scenarios in
864 Tunga-Bhadra river, India, *Hydrol. Process.*, 25, 3373–3386, <https://doi.org/10.1002/hyp.8057>, 2011.

865 Rehana, S. and Mujumdar, P. P.: Climate change induced risk in water quality control problems, *J. Hydrol.*, 444–
866 445, 63–77, <https://doi.org/10.1016/j.jhydrol.2012.03.042>, 2012.

867 Richards, F. D., Hoggard, M. J., and White, N. J.: Cenozoic epeirogeny of the Indian peninsula, *Geochemistry*,
868 *Geophys. Geosystems*, 17, 4920–4954, <https://doi.org/10.1002/2016GC006545>, 2016.

869 Saha, K. R., Mooley, D. A., and Saha, S.: The Indian monsoon and its economic impact, *GeoJournal*, 3,
870 <https://doi.org/10.1007/BF00257706>, 1979.

871 Santos, A. C., Portela, M. M., Rinaldo, A., & Schaeffli, B. (2018). Analytical flow duration curves for summer
872 streamflow in Switzerland. *Hydrology and earth system sciences*, 22(4), 2377-2389.

873 Searcy, J. K.: Flowduration curves, *Man. Hydrol. U.S. Geol. Surv.*, 1959.

874 Sinha, J., Sharma, A., Khan, M., and Goyal, M. K.: Assessment of the impacts of climatic variability and
875 anthropogenic stress on hydrologic resilience to warming shifts in Peninsular India, *Sci. Rep.*, 8, 13833,
876 <https://doi.org/10.1038/s41598-018-32091-0>, 2018.

877 Sivapalan, M.: From engineering hydrology to Earth system science: milestones in the transformation of
878 hydrologic science, *Hydrol. Earth Syst. Sci.*, 22, 1665–1693, <https://doi.org/10.5194/hess-22-1665-2018>, 2018.

879 Smakhtin, V. U.: Smakhtin 2010- Low flow hydrology.pdf, *J. Hydrol. Hydrol.*, 240, 147–186,
880 [https://doi.org/10.1016/S0022-1694\(00\)00340-1](https://doi.org/10.1016/S0022-1694(00)00340-1), 2001.

- 881 Stewart, M. K. (2015). Promising new baseflow separation and recession analysis methods
882 applied to streamflow at Glendhu Catchment, New Zealand. *Hydrology and Earth System*
883 *Sciences*, 19(6), 2587-2603.
- 884 Tashie, A., Pavelsky, T., and Band, L. E.: An Empirical Reevaluation of Streamflow Recession Analysis at the
885 Continental Scale, *Water Resour. Res.*, 56, <https://doi.org/10.1029/2019WR025448>, 2020a.
- 886 Tashie, A., Pavelsky, T., and Emanuel, R. E.: Spatial and Temporal Patterns in Baseflow Recession in the
887 Continental United States, *Water Resour. Res.*, 56, <https://doi.org/10.1029/2019WR026425>, 2020b.
- 888 Tongal, H., Demirel, M. C., and Moradkhani, H.: Analysis of dam-induced cyclic patterns on river flow dynamics,
889 *Hydrol. Sci. J.*, 62, 626–641, <https://doi.org/10.1080/02626667.2016.1252841>, 2017.
- 890 Vogel, R. M. and Fennessey, N. M.: Flow-Duration Curves. I: New Interpretation and Confidence Intervals, *J.*
891 *Water Resour. Plan. Manag.*, 120, 485–504, [https://doi.org/10.1061/\(ASCE\)0733-9496\(1994\)120:4\(485\)](https://doi.org/10.1061/(ASCE)0733-9496(1994)120:4(485)), 1994.
- 892 Vogel, R. M. and Fennessey, N. M.: Flow Duration Curves II: a Review of Applications in Water Resources
893 Planning, *JAWRA J. Am. Water Resour. Assoc.*, 31, 1029–1039, [https://doi.org/10.1111/j.1752-](https://doi.org/10.1111/j.1752-1688.1995.tb03419.x)
894 [1688.1995.tb03419.x](https://doi.org/10.1111/j.1752-1688.1995.tb03419.x), 1995.
- 895 Wagener, T., Blöschl, G., Goodrich, D. C., Gupta, H. V., Sivapalan, M., Tachikawa, Y., Troch, P. A., and Weiler,
896 M.: A synthesis framework for runoff prediction in ungauged basins, in: *Runoff Prediction in Ungauged Basins*,
897 Cambridge University Press, 11–28, <https://doi.org/10.1017/CBO9781139235761.005>, 2013.
- 898 Ye, S., Yaeger, M., Coopersmith, E., Cheng, L., & Sivapalan, M. (2012). Exploring the physical controls of
899 regional patterns of flow duration curves—Part 2: Role of seasonality, the regime curve, and associated process
900 controls. *Hydrology and Earth System Sciences*, 16(11), 4447-4465.
- 901 Yokoo, Y. and Sivapalan, M.: Towards reconstruction of the flow duration curve: Development of a conceptual
902 framework with a physical basis, *Hydrol. Earth Syst. Sci.*, 15, 2805–2819, [https://doi.org/10.5194/hess-15-2805-](https://doi.org/10.5194/hess-15-2805-2011)
903 [2011](https://doi.org/10.5194/hess-15-2805-2011), 2011.
- 904